NO. 118
CAS/CHEM-29-88

VIRGINIA TECH
CENTER FOR ADHESIVE AND SEALANT SCIENCE

NAG-1-300

FINAL REPORT

A FUNDAMENTAL APPROACH TO THE STICKING OF INSECT RESIDUES TO AIRCRAFT WINGS

BY

O. YI, N. S. EISS AND J. P. WIGHTMAN

VIRGINIA POLYTECHNIC INSTITUTE AND STATE UNIVERSITY

216 NORRIS HALL
BLACKSBURG, VIRGINIA 24061

Telephone: (703) 961-6824
TLX: EZLINK 9103331861
VPI-BKS

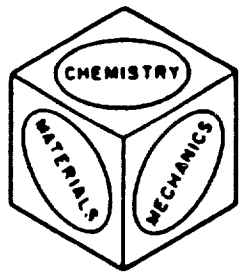

FINAL REPORT

INVESTIGATION OF FACTORS AFFECTING THE STICKING OF INSECTS ON AIRCRAFT WING SURFACES

BY
O. YI, N. S. EISS AND J. P. WIGHTMAN

PREPARED FOR
NATIONAL AERONAUTICS AND SPACE ADMINISTRATION

NASA – Langley Research Center
Transonic Aerodynamics Division
Hampton, VA 23665
D. M. Somers
Grant #NAG–1–300

from

Chemistry and Mechanical Engineering Departments
Virginia Polytechnic Institute and State University
Blacksburg, VA 24061

September, 1988

Investigation of Factors Affecting the Sticking of Insects on Aircraft Wing Surfaces

The aircraft industry is concerned with the increase of drag on planes due to the sticking of insects on critical airfoil areas. The objectives of the present study were to investigate the effects of surface energy and elasticity on the number of insects sticking onto the polymer coatings on a modified aircraft wing and to determine the mechanism by which insects stick onto surfaces during a high-velocity impact. Analyses including scanning electron microscopy (SEM), electron spectroscopy for chemical analysis (ESCA) and contact angle measurements of uncoated and polymer-coated aluminum surfaces have been performed. An air-gun was designed to accelerate insects to high speeds and impact them onto modified wing surfaces in a laboratory environment.

A direct relation between the number of insects sticking on a sample and its surface energy was obtained. Since the sticky liquid from a burst-open insect will not spread on the low energy surface, it will ball up providing poor adhesion between the insect debris and the surface. The incoming air flow can easily blow off the insect debris thus reducing the number of insects that remain stuck on the surface. Also a direct relation between the number of insect sticking onto sample surfaces and their moduli of elasticity was obtained. The deceleration of an insect impacting onto an elastomer reduces in proportional to the modulus of elasticity of the material. As a consequence, the rate of change of momentum is lower and the force and pressure exerted on the body of the insect is reduced if it impacts onto a material with a low modulus of elasticity. This lessens the chance of bursting the insect exoskeleton.

Contents

List of Figures

List of Tables

Chapter 1

Introduction and Overview

NASA's half-billion dollar Aircraft Energy Efficiency (ACEE) program, which started in 1976, is a jointly funded research and technology effort between NASA and industry [1,2]. Commercial jet aircraft energy consumption was the primary factor in the ACEE program, and the development and demonstration of advanced technologies applicable to transport aircraft has been mainly emphasized [3]. The ACEE program has focused on four aircraft technology areas: advanced aerodynamics, flight control, composite structures, and laminar flow [3].

Fuel has been the major portion of the direct operating cost for airlines. High fuel costs due to rapid increase in airline fuel prices, and commercial aviation fuel consumption have continued to cause serious financial problems for aircraft industries [3]. Due to other factors such as cost of capital, load factors, fuel efficiency, airline regulations, foreign competition, and environmental regulations, the ACEE airframe technology has become important [4].

1.1 Laminar Flow

One of the ACEE programs is the development of technology for viscous drag reduction through laminar flow. Higher fuel efficiencies in aircraft may be achieved using a wing design which has maximum aerodynamic efficiency by reducing drag and minimizing wing size and weight [5]. The essential condition for achieving a significant reduction of drag on the airplane is obtaining laminar flow over airfoil surfaces, which has no boundary layer separation, and an absence of turbulence. Laminar flow can be achieved either by the use of suction through the wing structure to remove the boundary layer (laminar flow control) or encouragement of natural laminar flow [3,6].

Suction for laminar flow control through the wing surface can be obtained by millions of holes created on the surface by an electron beam. A sufficiently smooth and wave-free surface is an essential factor in accomplishing laminar flow. The maintenance of wing-surface quality in normal service is also essential. With assistance from advanced material technology, smoothness required for a laminar flow control surface can be easily achieved, and the fuel savings for a laminar flow control aircraft would be approximately 20% to 22% [6].

1.2 Wing Contamination of Laminar Flow Control Airfoils

A smooth leading edge is essential for maintaining laminar flow. Roughness created on the leading edge by icing, frost and insects have a great affect on the boundary layer at the leading edge, where a allowable height of roughness particle size is only between 0.10 and 0.15 mm [5,7]. Roughness in the laminar flow-region of an airfoil interrupts smooth laminar flow and promotes a transition from laminar to turbulent flow by creating eddies, while roughness in the turbulent region increases the turbulent friction coefficient which in turn increases the drag coefficient [7].

Luers [7] stated that the roughness due to icing and frost on the airfoil not only reduces performance but also threatens aircraft safety. Ice accretion on the wing can be dangerous when the plane enters into a cloud of supercooled water droplets, while frost can cause danger during take-off. Because of their roughness and the shape change produced on the airfoil, freezing ice and rain and a heavy layer of frost have caused a large number of aviation accidents. For example, 49 general aviation accidents in 1979 were mainly caused by icing.

1.2.1 Wing Contamination due to Insect Debris

Although roughness due to insect debris collected on the leading edge is not a safety problem, decrease in performance has been of great concern. Insect contamination usually occurs on aircrafts at low altitudes below about 152 m corresponding to take-off and initial climb [8,9]. These insects remain on the leading edge of the wing causing an early transition of the laminar boundary layer to turbulence during cruise flight. A significant increase in drag occurs and the fuel savings expected for laminar flow can not be achieved [10].

An insect consists of many different chemical compounds [11-13], but it is unnecessary to discuss details of their chemistry herein. These compounds determine the spreading and adhesion of the burst-opened insect body on a solid surface. When the insect impacts a surface, the stress causes the cuticle of the insect to crack or split. Depending on the mechanical properties of the insect cuticle, the impacting force will have different effects on the insect body.

The cuticle of an insect functions as an exoskeleton and as a barrier between the living tissues and the environment [14]. The cuticle is most prominently a skeleton, which consists of complex composite materials [15]. The mechanical properties of such composites depend on the individual properties and interaction of components. The tensile properties of some insect cuticles have been studied by Hepburn *et al.* [15-20]. It was found that most insect cuticles are stiff, highly plastic, or intermediates between these two. The stiff cuticles, which

shows high relative stiffness, high tensile modulus and low breaking strains, usually fail in tension [14,15]. On the other hand, the plastic cuticles, which exhibit very low relative stiffness, low tensile modulus and large breaking strain, usually fail in shear.

The insect population above an area of agricultural land was studied by Freeman [21] from just above ground-level to nearly 91 m The following conclusions were reported:

1. The population consisted mainly of small weak flying and low weight insects which drift involuntarily with the wind.

2. The local vegetation determined the general character of the aerial fauna, which showed significant changes from month to month.

3. The largest numbers and variety of insects were found in May, June, and September, active times in mating and dispersal.

4. Maximum numbers of most groups of insects occurred at relative humidities below 59%, wind velocities of 19 km/hr, and below and at temperature in excess of 18°C.

Since there were significant changes in types of insects from month to month and one location to another due to vegetation, any systems developed must be capable of preventing varieties of insects from sticking.

1.2.2 Insect Reduction Studies

There have been a number of methods attempted to minimize the sticking of insects on airfoils. Gray and Davies's [22] solution was to cover the front part of the test section with a sheet of paper stretched tightly around the leading edge. After the aircraft reached an altitude higher than 152 m, the pilot discarded the paper by pulling a string looped through the paper.

Wortmann's [23] solution to overcome the insect contamination problem was to use an elastic surface such as solid rubber or foam rubber. At high velocities, even small objects such as insects posses sufficient kinetic energy to cause their bodies to burst open upon impact, and the viscous body fluid will adhere to the surface. An elastic surface can store the impact energy of an insect for a short period of time and push the insect away from the surface. In such a process, the bursting open of the insect and adhesion of the insect debris to the surface may be prevented. Wortmann also found that as thickness of the rubber increases, the elasticity gets more effective even at the high velocities investigated.

Several different materials such as Teflon^R tape, spray-on Teflon^R, organic-silicon hydrophobic coating, random rain-repellent coating, and polished aluminum alloy were tested [5,10]. Although none of these materials were able to prevent the adherence of insect debris, insects remaining on the Teflon^R surface were easily removed with a damp cloth applying only a light pressure [10].

Spray systems which are also suitable for anti-icing control, have been investigated for effectiveness in controlling insect debris build-up [5,10]. A study has been done with a liquid mixture of water and anti-freeze where the liquid is continuously ejected onto the wing surface during take-off or landing to prevent insect adhesion [24]. Although this method has some potential, there are disadvantages due to the requirements of maintenance and of a continuous liquid supply. Another potentially interesting scheme is the cryogenic frost system. This system can provide cold air (approximately -15°C) along the leading edge, and the cold metal would (except in dry atmosphere) cause the formation of frost, in a short period of time [24]. Thus, the adhesion of insects during take-off and climb can be prevented by a frost coating, and the airstream would quickly melt the frost and leave a clean surface for laminar flow. However, ground preparation for following flights require manual cleaning of the leading edges, since the cryogenic frost system is not effective during landing.

Shielding the wing surface from insects using a leading edge flap has also been successfully

tested [5]. Sublimation coatings, mechanical scrapers, and deflectors were also investigated in the past [24].

Siochi, *et al.* [25] studied the effects of surface energy and surface roughness on the adhesion of insects debris on the modified airfoils. Four polymer samples (Nyebar^R, Teflon^R, polysulfone and polymethylmethacrylate) with different surface energies were investigated by impacting insects in a road test. Fewer number of insects were found on the lowest surface energy polymer (Nyebar^R) than on the highest energy surface (polysulfone). It was concluded that the surface energy of the polymer used had an effect on the number of insects sticking to the surface while the effect of surface roughness was insignificant.

Chapter 2

Scope of the Study

2.1 Objectives of the Study

The objective of the present study was to investigate factors such as elasticity and surface energy of polymers which might affect the insect fouling of modified airfoil surfaces under controlled conditions. Insect-sticking mechanisms on different sample surfaces could also be obtained. Finally, surface analysis such as electron spectroscopy for chemical analysis (ESCA), scanning electron microscope (SEM), and contact angle measurements using a goniometer were applied on aluminum and test polymer surfaces to determine their surface energy, composition, and topography.

2.2 Plan of the Study

The priminary focus of the present study was to simulate the impact of insects on the sample surface without introduction of a large experimental error. The study was divided into three phases depending on the method used to collect insects. A modification and

a new technique were developed, as any experimental error was assumed to be associated with a given insect collecting method.

2.2.1 Phase I Study Using the Established Road Test

The effectof surface energy on the number of insects sticking has been extensively studied by Siochi *et al.* [25,26]. The results of the study indicated that on average, fewer insects stuck onto lower energy surfaces. However, the total reduction over the range of surface energies examined was small as shown in Figure 1. In addition, results from individual polymers used showed large deviations from the average trend, and errors associated with each point were often larger than the average reduction of surface energies studied. Such results might be due to problems associated with road testing. There were probable experimental errors which might have been introduced during the road test. One source of error might be a variable insect flux across the sample holder so that the number of insects striking one sample might be different from that striking an adjacent sample. A larger number of tests might have been required simply to eliminate such statistical errors. It is also possible that uncontrollable sizes and types of insects, which may have different effects on different samples, contribute experimental errors. It was essential that such potential errors be determined before further research was performed.

The objectives of the phase I study were to investigate the feasibility of the established road test and to test different set of samples from ones tested by Siochi *et al.* [26].

2.2.2 Phase II Study Using a Modified Road Test

The first objective of this phase of the study was to detect possible experimental errors described in the phase I study from an investigation of insect distribution across the sample holder (half-cylinder). The second objective of the study was to develop a new sample arrangements so that further use of the road test was possible. The last objective was to

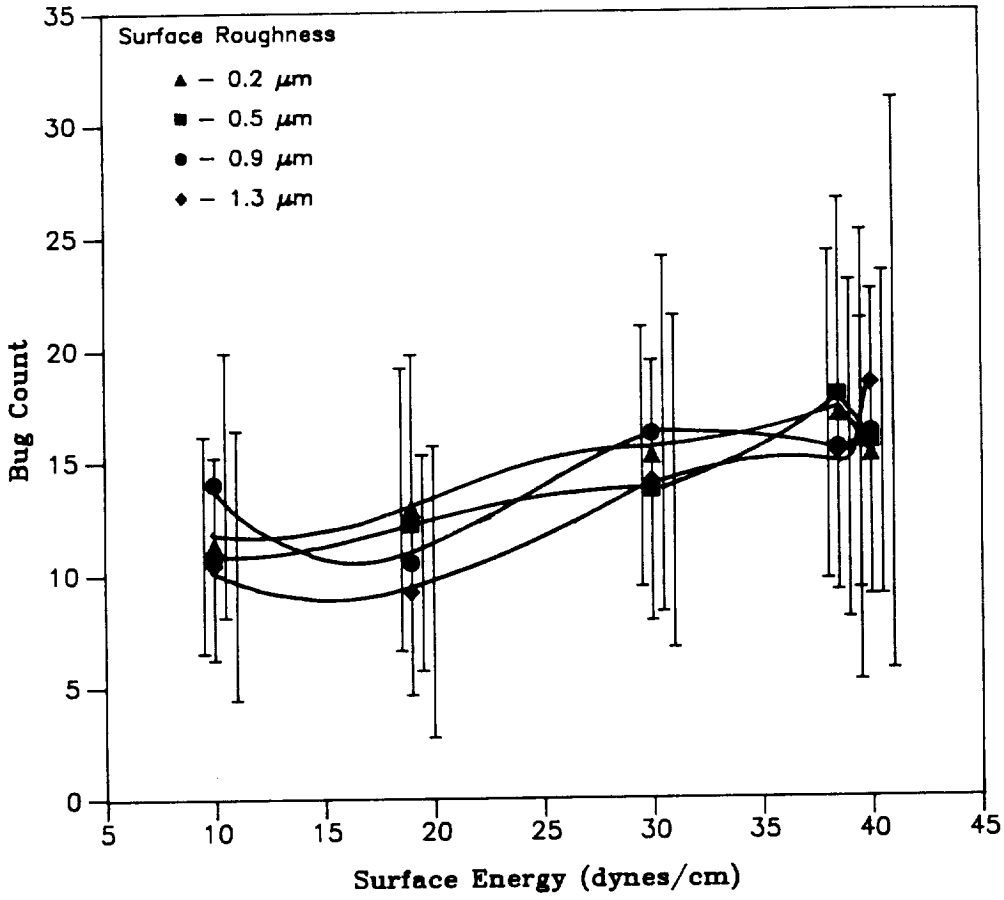

Figure 1: **Bug count versus surface energy obtained by Siochi *et al.*:** The results plotted in this figure are obtained from the road tests by Siochi *et al.* [26]. It is noticed that absolute numbers of insects sticking on substrates are compared, instead of their normalzied percentages.

study the elasticity effect of polymer-coated metal surfaces (modified aircraft wing surfaces) on the insect adhesion using the modified road test with the new sample arrangement.

Although a modified road test could reduce some errors due to a variable insect flux, a large number of runs per sample might still be required. Other serious problems with any road test are limitations imposed by weather conditions (no experiments were possible during cold or rainy days), and errors due to uncontrollable sizes and types of insects.

2.2.3 Phase III Study Using an Air-Gun

A new insect impacting technique, which could overcome problems associated with the road tests described in the previous paragraphs, was needed. An air-gun, which was able to accelerate insects up to 65 mph (speed of car during the road tests) or higher was assembled to perform experiments without limitations of weather, and under controlled conditions. Another advantage of the air-gun was the use of a single type of insect having a constant size. Different types of polymer samples could be investigated using the air-gun and a single type of insect could be used to study the effects of elasticity and surface energy on the insect adhesion.

Chapter 3

Experimental

3.1 Insect Impact Studies

The preliminary focus of the present study was the development of a technique to study the impact of insects on the sample surface without introducing a large experimental error. As described in Chapter 2, the study was divided into three phases depending on the method used to collect insects.

3.1.1 Materials Tested in this Study

Polymer samples tested in this study are described below.

Fluorocabon Elastomer (FCE) —Five different types of fluorocarbon elastomers (FCE's) received from 3M were tested in phase I and II studies using the road tests. FCE samples are 2.15 mm thick and have different fluorine contenet with different mechanical properties. Two of FCE samples, designated as A & B contain 69% fluorine and ones designated as C, D & E contain 66 % fluorine. Their moduli of elasticity at 200 % elongation vary from 972 to 2,900 kPa.

Neoprene and Viton^R —Neoprene and Viton^R samples both 2.00 mm were obtained from duPont and used in both phase I and II studies.

Polyurethane —Polyurethane films were pressed from estanes (Goodrich) with 31% hard segments in 152.4×152.4 mm molds with thickness of 0.79 mm and 1.59 mm at 150°C and 190°C, respectively. Because they were pressed at two different temperatures, their moduli of elasticity are different.

Styrene Butadiene Rubber (SBR) —Four 2.00 mm thick styrene butadiene rubber (SBR) samples obtained from U. S. Army -Fort Belvoir were tested during the phase II road test study. Their moduli of elasticity at 200% elongation vary from 4,780 to 5,060 kPa.

Teflon^R Samples —Teflon^R fluorinated ethylene propylene copolymer (FEP) and tetrafluoroethlene copolymer (TEFZEL) both with thicknesses of 0.01 mm, and 0.02 mm thick TR-Tedlar^R poly vinyl fluoride (PVF) were obtained from duPont. Pumbling quality Teflon^R tape with a thickness of 0.06 mm, and 0.12 mm thick Teflon^R films were tested mainly during the phase III study using the air-gun.

Others —Hostaphan^R polyester and polyethylene films with thicknesses of 0.02 mm, and 0.03 mm thick polypropylene were obtained from Rexham. These three samples and 0.02 mm thick polycarbonate and 0.01 mm thick chlorotetrafluoroethylene films and Nyebar^R barrier film coating were investigated during the phase III study using the air-gun.

3.1.2 Phase I Study

The objective of the phase I study was to investigate the reliability of the established road test [26] to obtain reproducible results.

3.1.2.1 Samples Tested and Their Preparation

The samples tested in the phase I study were five FCE's, neoprene, Viton^R, and polyurethanes with two different thicknesses, which have different moduli of elasticity. There was the definite possibility of contamination on the elastomer surfaces due to grease during pressing and handling. All the elastomers were washed in a commercial detergent (Tide^R) in water, and subsequently rinsed with deionized water at least 10 times. The washed elastomers were dried over-night in a vacuum oven at room temperature.

Five 19×152 mm strips of each elastomer were washed and dried as described above, and adhesively bonded to 25×203 mm aluminum strips. To remove any grease from the contact surfaces, the aluminum surfaces were wiped with Kemkit^R wetted with acetone and the contact surfaces of elastomers were washed with pure ethanol.

Adhesives from the Lord Chemical Corporation were used to glue the elastomer strips to the aluminum substrate. Viton^R, polyurethane and FCE strips were glued to the aluminum strips using Chemlock (cyanoacrylate adhesive), and pressed between two aluminum strips for at least 30 seconds while the adhesive cured. Neoprene strips were glued using Chemlock 234B (mixture of xylene, trichlorethylene, and carbon black), and pressed between two aluminum strips. The ends were clamped and placed in an oven at 82.2°C for two hours. All washed elastomers were stored in the dessicator over a drying agent Drierite^R.

3.1.2.2 Insect Impact -Road Test

Insects impact studies were done using the road test previously designed by [26]. The sample strips prepared as described above and five aluminum (control) strips were randomly mounted on either an aluminum or a PVC half cylinder (102 cm long and 10 cm or 13 cm outer diameter) as shown in Figure 2. These cylinders were then mounted as shown on the top of a car and driven at average speed of 89 km/hr) around a loop on Route 618 in

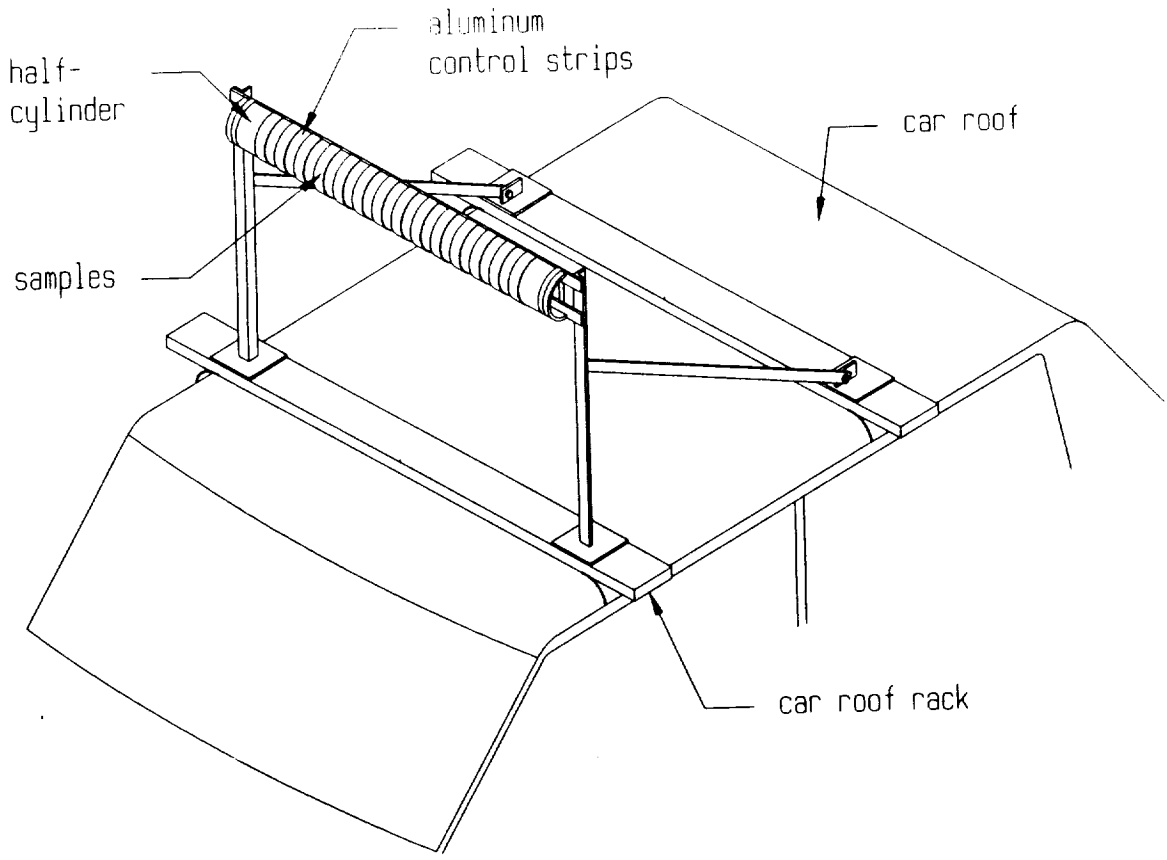

Figure 2: **Simplified diagram of an insect collecting device:** Sample and control strips were randomly mounted on a half-cylinder which was then mounted on a top of the car. Insects were collected on the sample and aluminum surfaces by driving at average speed of 89 km/hr.

Gloucester County, Virginia between 19:05 and 20:20 hrs on September 7, 1986 to impact insects on the polymer and aluminum surfaces. The insects collected on all the samples and aluminum were counted visually and summed.

3.1.3 Phase II Study

A large experimental error was assumed to be introduced during the road tests performed in phase I study caused by a variable insect flux. Variation in the insect flux might be due to a random distribution of insects on the road, the effects of wind, and possibly other road traffic. To detect the presence of such errors, the insect distribution across a half-cylinder mounted on the top of a car using only aluminum strips was studied. The relationships between the number of insects sticking on the sample surfaces and properties of the polymer samples such as modulus of elasticity and surface energy were investigated using a new arrangement of samples and control.

3.1.3.1 Insect Flux Across the Half-Cylinder

To determine the presence of experimental error due to a variable insect flux as described above, road tests conducted carried on three different days during the summer season driving from Blacksburg, Virginia to Princeton, West Virginia and back, a total distance of approximately 161 km at average speed of 89 km/hr. Twenty 25×229 mm aluminum strips were mounted on a 102 mm OD (outside diameter) half cylinder which was then mounted on the top of a car. The number of insects sticking on each strip were counted visually and recorded. By comparing the number of insect sticking on each aluminum strip, the insect density distribution across the half-cylinder was obtained.

3.1.3.2 Samples Tested and Their Preparation

The five FCE samples tested in the phase I study and four SBR samples were tested to study the relationship between the modulus of elasticity and the number of insect sticking to the elastomer. Since all four SBR samples or five FCE samples are expected to posses a similar surface energy, this factor is eliminated in comparing between the number of insect sticking on the elastomers. Thirteen 19×152 mm strips of each FCE were washed, dried and adhesively bonded with cyanoacrylate to 25×229 mm aluminum strips as described in the phase I study. Six 19×152 mm strips of each SBR were adhesively bonded to 19×229 mm aluminum strips with cyanoacrylate. Both surfaces were washed by wiping with Kemkit^R wetted with acetone before the adhesive was applied. The test surfaces of SBR strips were washed by gentle wiping with Kemkit^R wetted with acetone as suggested by personnel at the Fort Belvoir research laboratory.

Plumbing-quality Teflon pipe thread tape (Teflon^R tape) was also investigated. Twenty 19×152 mm strips of Teflon^R tape were attached on 25×229 mm aluminum strips using spongy 3M Scotch double-sided mounting tape (approximately 1.23 mm thick). Another twenty strips of Teflon tape were glued on aluminum strips with non-spongy 3M double-stick tape (approximately 0.01 mm thick).

3.1.3.3 Insect Impact -Modified Road Test

It was determined that the insect distribution across the half-cylinder used during the road tests was nonuniform as explained in detail in the following chapter. The sample and aluminum strips used in the phase I study were mounted in a random manner for each road test. However, this method could lead to serious experimental error since some strips of any one type of sample might be mounted in a position where the insect flux may be low or high. This leads to variations in the number of insects on different strips of a given sample, and to inaccuracies in calculating statistical averages based on five strips of one sample. The

chance of mounting a sample at a high or low insect flux position can be reduced by running a road test with only one type of sample with an equal number of aluminum controls.

The sample and control strips were mounted on the aluminum half-cylinder as shown in Figure 3, and the road tests were performed at the times and dates listed in Table I driving from Blacksburg, Virginia to Glen Lyn, Virginia and back, a total distance of approximately 161 km at average speed of 89 km/hr. The number of insects on each strip was counted visually and summed. Instead of comparing the absolute numbers of insects on different samples, normalized percentages (NP) which compare the number of insects sticking onto a given sample with that sticking onto aluminum were calculated by the following equation:

$$\text{NP} = \frac{\text{total number of insects on sample strips}}{\text{total number of insects on aluminum strips}} \times 100 \qquad (3.1)$$

This allowed running one type of sample per run with aluminum control strips, and gave an indication of the effectiveness of that sample type in reducing the number of insect sticking to the surface. A NP value of 20% means that there is an 80% fewer insects sticking on a given sample than onto aluminum.

3.1.4 Phase III Study

Several possible errors introduced during road tests and problems associated with the insect-impacting simulation using road tests were described in Chapter 2. A new insect impacting technique using an air-gun was developed and tested to overcome such problems. The air-gun could accelerate insects up to 105 km/hr or higher and experiments could be performed without limitations of weather and under controlled conditions. The effects of elasticity and surface energy on the insect adhesion were extensively studied using the air-gun.

3.1.4.1 Review of Fluid Flow in a Circular Pipe

If the shear force per unit area of any fluid is proportional to the negative of the local velocity gradient, then the fluid is defined as a Newtonian fluid. All gases and most simple

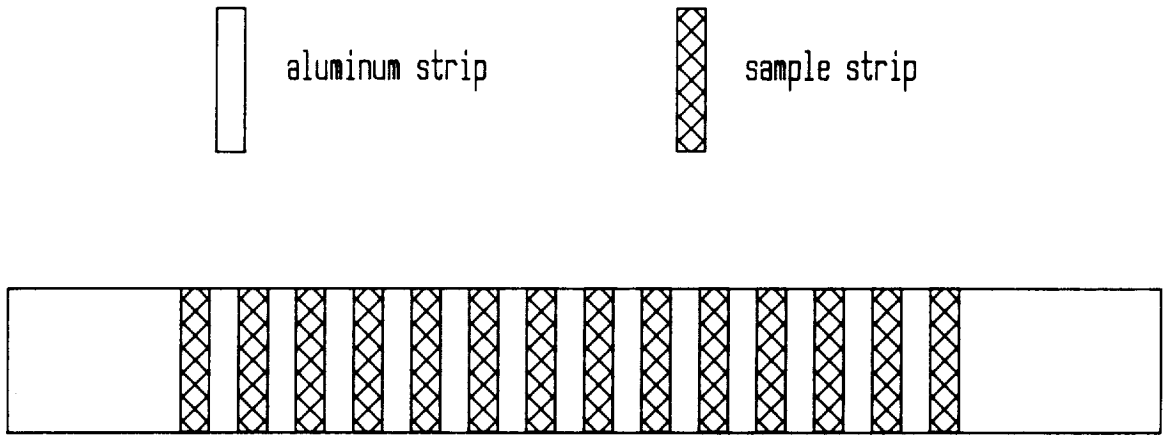

Figure 3: **A new arrangement of sample and aluminum strips across the half-cylinder:** To reduce the chance of mounting a sample at a high or low insect flux position, a road test was performed with only one type of sample with an equal number of aluminum strips.

Table I: **Dates and Times of the Phase II Road Tests.**

Sample	Date (1987)	Time
FCE–A	August 6	19:45 – 21:30
FCE–B	August 9	20:00 – 21:45
FCE–C	August 10	20:10 – 21:45
FCE–D	August 11	19:30 – 21:32
FCE–E	September 2	19:17 – 20:48
SBR–3C	September 3	19:37 – 21:15
SBR–7C	September 3	19:37 – 21:15
SBR–26	September 8	19:33 – 21:00
SBR–17B	September 8	19:33 – 21:00

liquids are Newtonian fluids[27]. The axial velocity profile of the flow through a circular tube can be obtained by the equation of motion in cylindrical coordinates for a Newtonian fluid from a momentum balance and Newton's law of viscosity. For this derivation, constant density and viscosity of the fluid that are independent on the radial position in the tube are assumed. The circular tube must be long enough so that end effects can be ignored; and a steady state air flow must be achieved so that the velocity v_z is only a function of radial position in the tube.

The dimensionless Reynolds Number (Re) for flow in a circular tube is defined as[28]:

$$Re = \frac{D < v_z > \rho}{\mu} \tag{3.2}$$

where

D = tube diameter

$< v_z >$ = average axial velocity

ρ = fluid density

μ = fluid viscosity

The flow in a very smooth circular tube is laminar when the value of Re is less than 2,100 and turbulent when Re is greater than 2,100 [27]. The velocity of the turbulent flow fluctuates over a period of time about a mean value, so that the time-smoothed velocity by taking an average of velocity over a time interval is considered. In the immediate region of the tube wall, the velocity fluctuations in the axial direction are greater than in the radial direction. Newton's law of viscosity is used to describe the fluid flow as a function of radius. As the distance from the tube wall increases (approaching the center of the tube), the velocity fluctuations are very random and turbulent flow is fully developed[27].

For both types of flow (laminar and turbulent) the velocity distributions over a tube cross section develop as shown in Figure 4. Thus, the axial velocity (v_z) is a function of radius

(r), and the average axial velocity is obtained by:

$$< v_z >= \frac{\int_0^{2\pi} \int_0^R v_z(r)\, dr d\theta}{\int_0^{2\pi} \int_0^R r\, dr d\theta} \tag{3.3}$$

where R is the radius of the tube and $v_z(r)$ is the axial velocity which is a function of r. As shown in Figure 4, the velocity distribution over a tube cross section for turbulent flow is more uniform than for laminar flow.

3.1.4.2 Preliminary Study of the New Insect-Impact Technique

Insect Impact Technique To determine the feasibility of using a controlled insect impacting method, an air-gun was designed and tested. The air-gun consisted of a 25 mm PVC pipe, a T-connector, and a nozzle arranged as shown in the simplified diagram in Figure 5. Compressed air was passed through the nozzle, and the high velocity air exiting from the nozzle created a suction behind the nozzle that induced a large inflow of air through the feed chute. This large volume of air was accelerated as it flowed past the nozzle creating a high velocity flow of air in the down stream section of the pipe. Any small object, such as an insect, that was placed in the feed chute would be sucked into the pipe, accelerated in the pipe, and ejected from the end of the pipe at high velocity. The position of the nozzle along the pipe axis is very critical, since it will determine the amount of air sucked into the pipe. The optimum position of the nozzle, which gave the miximum air velocity inside of the pipe, was determined by measuring air velocity at the exit end of the pipe while varying the nozzle locations.

Determination of the Velocity The exact velocity of an object exiting from the end of pipe was determined using a camera, a light spherical particle, and a strobe lamp. In a completely dark environment, the light reflected from a small white object located approximately 152 cm from a camera and illuminated by the strobe lamp operated at 400 Hz could

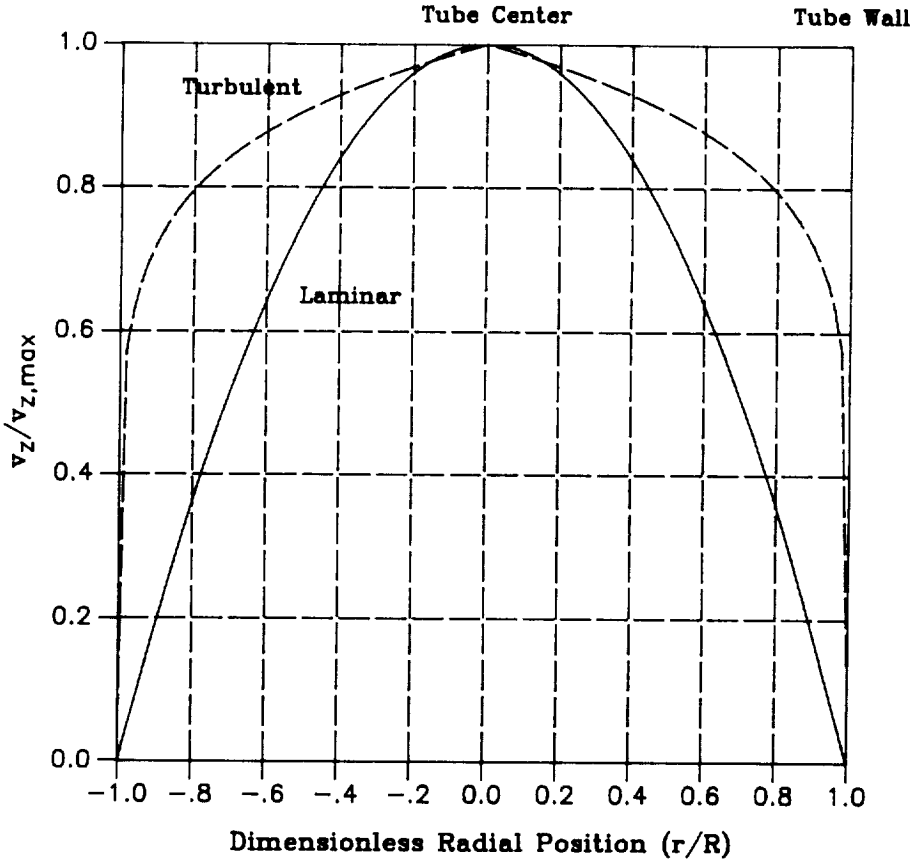

Figure 4: **Laminar and turbulent velocity profiles:** Qualitative comparison of laminar and turbulent dimensionless velocity distributions ($\overline{v}_z/\overline{v}_{z,max}$) in a circular pipe as a function of dimensionless (r/R) radial position [27].

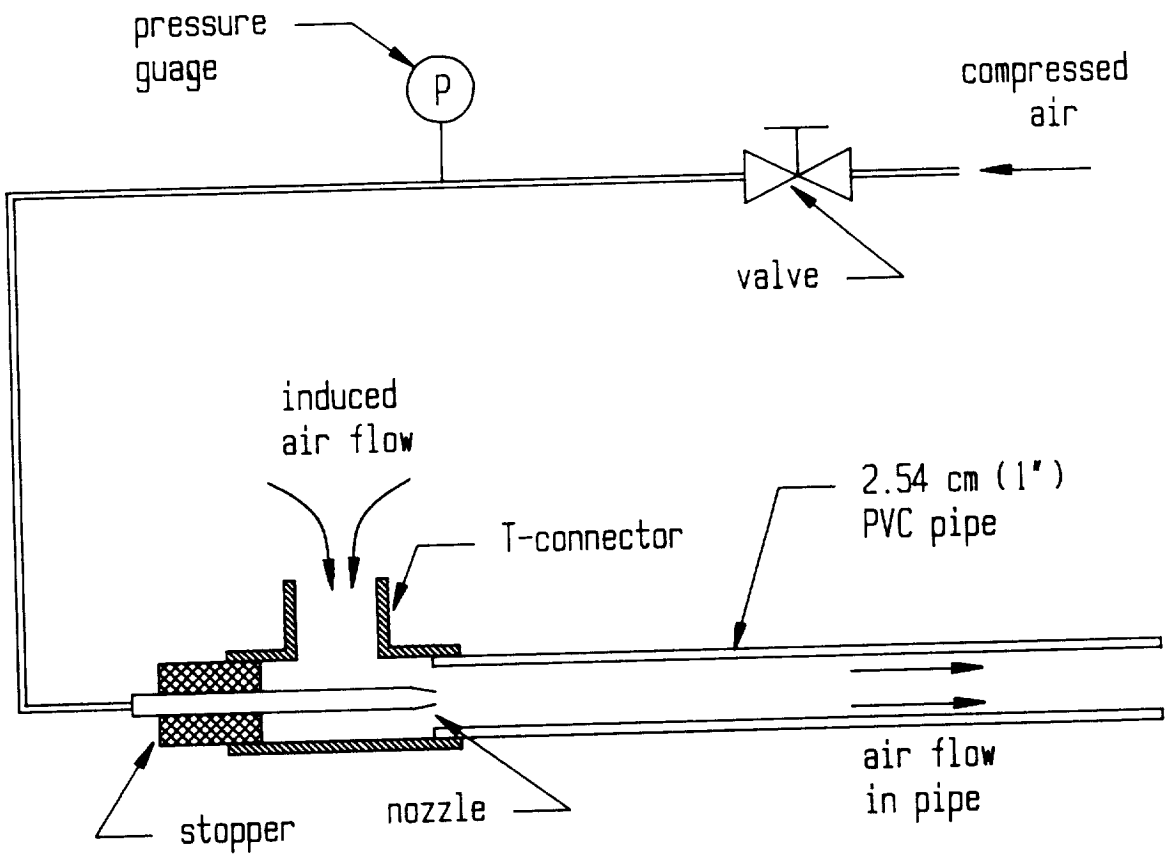

Figure 5: **Simplified diagram of air-gun:** Compressed air, passed through a nozzle created a suction behind the nozzle that induced a large inflow of air through the feed chute. An insect, placed in the feed chute is sucked into the pipe and accelerated so it exits from the end of the pipe at a high velocity.

be recorded on 3200 ASA film. Spherical polyethylene particles (approximately 10 mm diameter) - were coated with chrome to achieve maximum reflection of light. The experiment was carried out in darkness with illumination of the particles provided by a strobe lamp. A 35 mm camera was focused on the plane of the path of the particles exiting from the end of the pipe. A sheet of black velvet was placed approximately 183 cm from the camera, and behind the path of the particles to create a dark background. The position of the strobe lamp required adjustment until the brightest image of the particle appeared in the camera viewfinder without light reflected from other surfaces interfering with the image. The final set-up of the apparatus is shown in Figure 6.

First a ruler placed along the path of particles exiting the pipe was photographed using a constant (un-strobed) light source. Then keeping the position of the camera fixed, photographs of exiting particles were obtained with strobed lighting on successive frames of film. When a particle was dropped into the feed chute, the shutter of the camera was opened, and as a particle exited the end of the pipe it formed images on the film as it crossed the path of the strobed light. Since the light from the strobe was fired at a fixed frequency, the particle appeared as a sequence of equidistant bright dots as shown in Figure 7. The actual distance between two dots was calculated by measuring the distance between two successive dots appearing in a photograph and scaling up by the ratio between the actual distance indicated by the ruler and the distance measured in the photographs of the ruler. From the distance between successive dots and the frequency of the light from the strobe lamp, the velocity of the particle, v_p was calculated by:

$$v_p = \text{distance between successive dots} \times \text{strobe frequency} \tag{3.4}$$

The average particle velocities from thirteen measurements using a compressed air supply of 35 kPa and from four measurements at 70 kPa were calculated to be 82 km/hr and 105 km/hr, respectively. Higher velocities could be obtained by increasing the pressure of the compressed air supply, with an available maximum of 517 kPa.

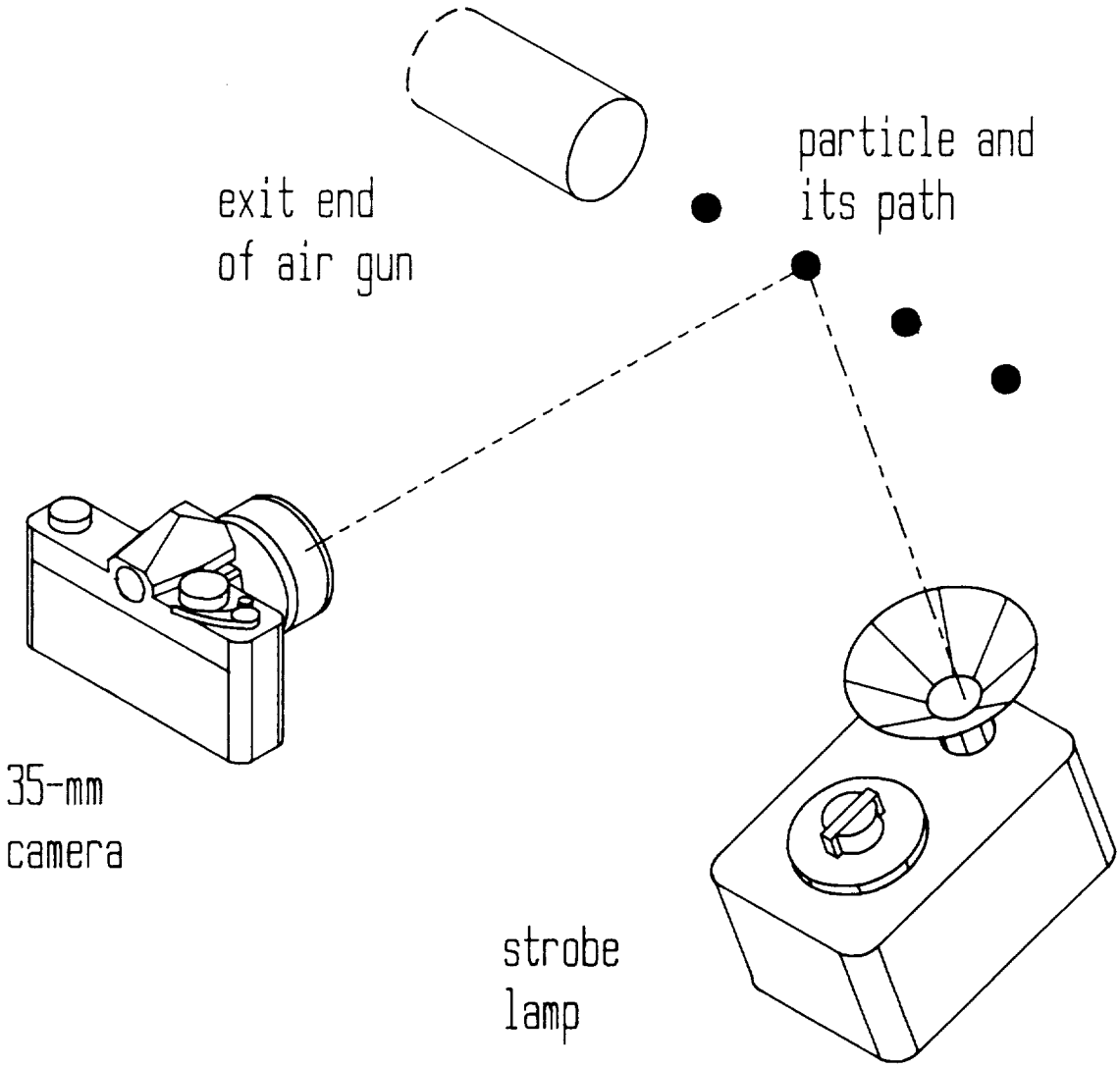

Figure 6: **Photographic technique used to determine the velocity of a particle exiting from the air-gun:** The particle exiting from the end of the pipe appeared as a sequences of equidistant dots, when the particle was illuminated by a strobe lamp in the dark environment. The path of the particle was photographed using a 35 mm camera.

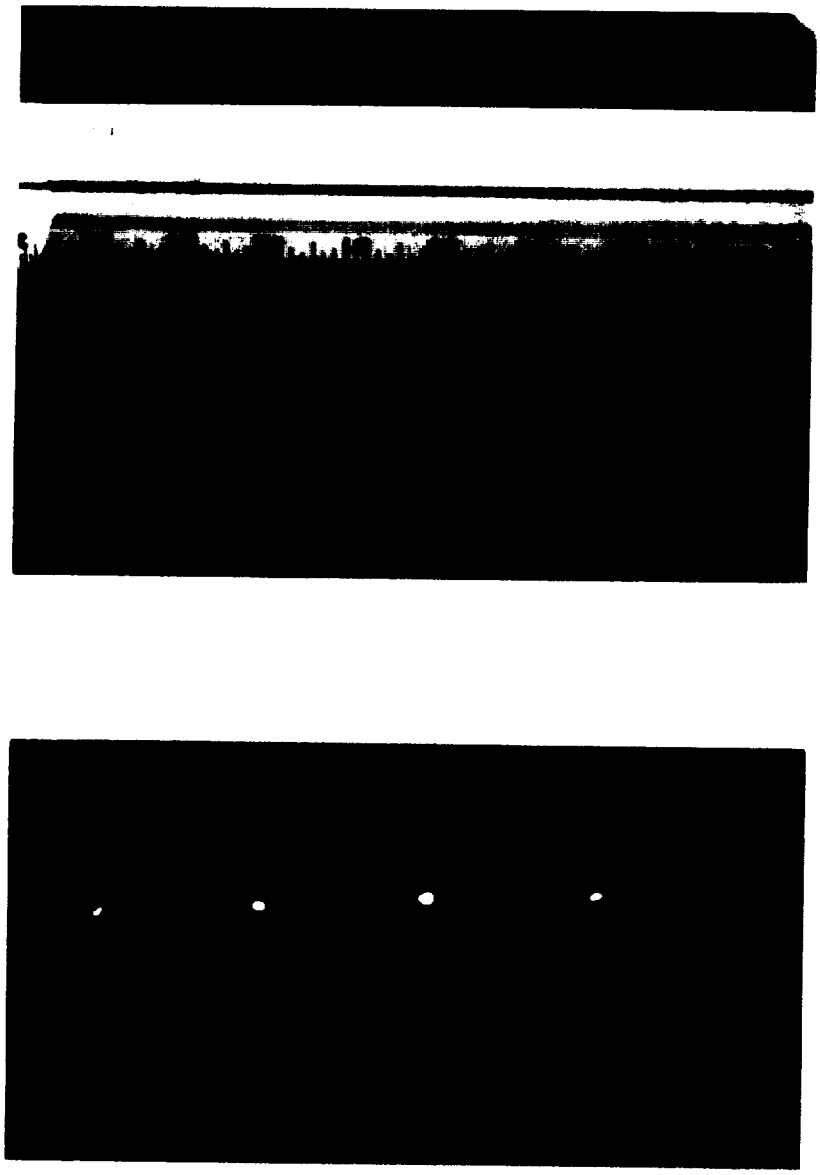

Figure 7: **Photographs of a ruler and a particle trace at 35 kPa:** The path of the particle exiting from the end of the pipe was illuminated by the strobe lamp as a sequence of dots. The velocity of the particle was calculated from the strobe frequency and the distance between successive dots.

3.1.4.3 Development of the Air-Gun

Since the velocity of the particle exiting from the end of the air-gun was determined to be reasonably high, using the air-gun as a controlled insect-impact device approved to be feasible. Further development of the air-gun was done to obtain more uniform velocity distributions over the entire sample target. A larger PVC pipe (length: 368.5 cm; diameter: 7.6 cm) was used. Increasing the diameter and the air velocity should increase the degree of turbulent flow creating a more uniform velocity distribution across the cross-section of the pipe. This caused insects within the pipe to impact the target with approximately the same velocity regardless of their radial position. The length of the pipe was increased so that the entrance effects would be negligible toward the exit end, and the air flow inside of the pipe would reach steady state. As shown in Figure 8, a 10.2 cm×20.3 cm×152.4 cm rectangular plexiglas duct was placed at the end of the circular PVC pipe, to prevent the air flow from the end of the circular PVC pipe from diverging into the environment. An additional amount of air was sucked into the gap between the circular and the rectangular pipes, and further improvement of the velocity distribution was achieved. The sample target - an aluminum strip which the polymer sample strips were glued onto was bolted on the sample holder as shown in Figure 9. This sample holder was placed at the center of the cross section of the rectangular duct along its axis and toward the exit where fully developed turbulent flow was present.

3.1.4.4 Determination of Air Profile and Velocity

A small quantity of finely powdered dry ice was poured into the feed chute and blown across the length of the air-gun to study the air flow profile inside the plexiglas duct. Since the density of dry ice is low and the particle size is small, the path of dry ice passing through the rectangular duct would be the same as that of the air flow. After the air flow was fully developed, a small quantity of dry ice was introduced into the feed chute and its path was observed.

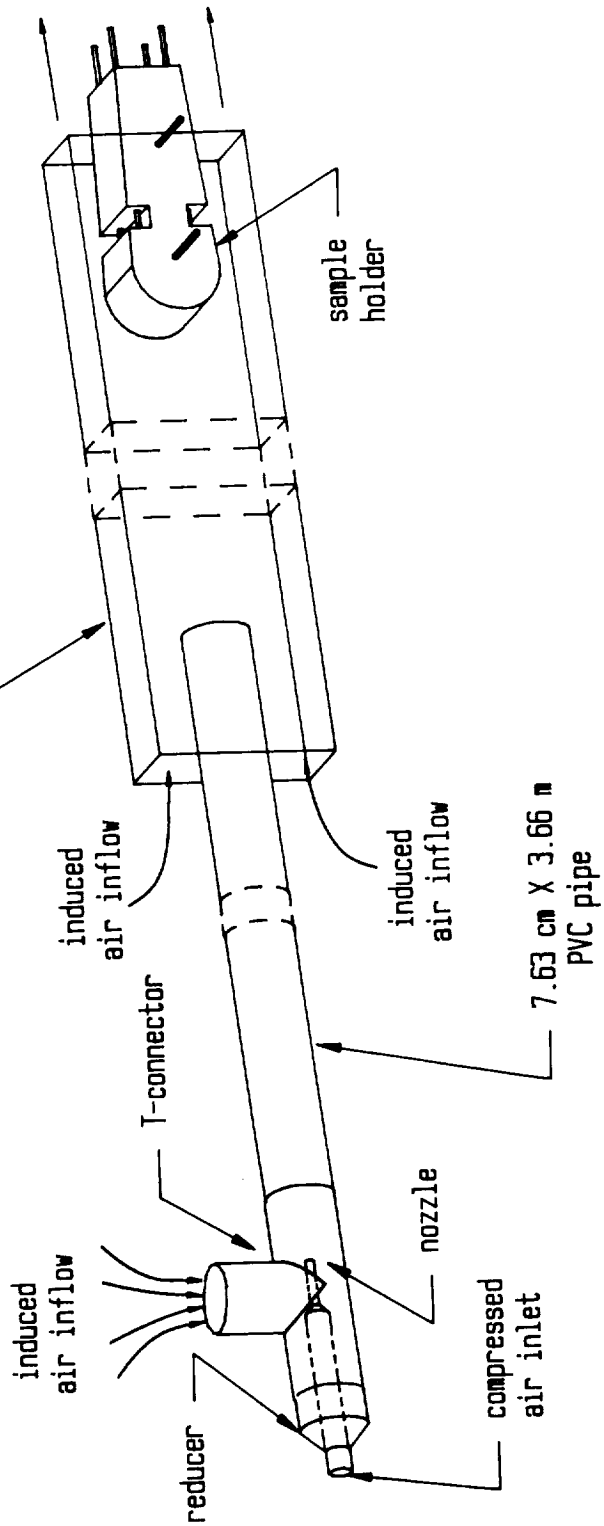

Figure 8: **Simplified diagram of improved air-gun:** Increasing the diameter of the circular pipe increases the degree of turbulent flow, creating an uniform velocity distribution across the cross-section of the pipe. The entrance effects become negligible toward the exit end of the circular pipe. The plexiglas duct prevents the air flow exiting the circular pipe from diverging, and also induces an extra flow of air into the system.

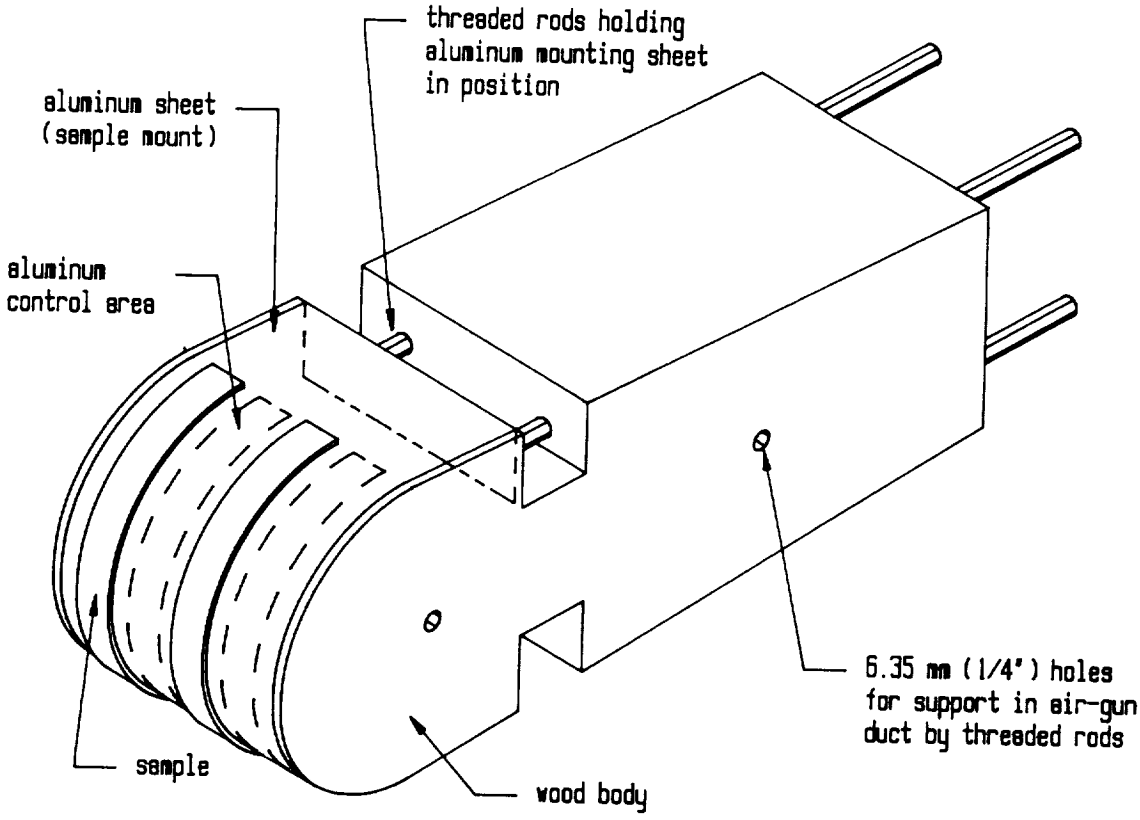

Figure 9: **Sample holder used in the air-gun:** Sample strips were mounted onto the aluminum strip which then was bolted onto the sample holder.

As shown in Figure 10, no flow was seen close to the walls of the duct even at the exit. The expansion of air from the 7.63 cm PVC pipe into the rectangular duct would induce an additional flow of air into the duct as illustrated in Figure 8. The study of the stream lines showed that the eddies created by this air flow entering the high velocity stream from the PVC pipe were quickly dampened and had no effect towards the exit end of the duct.

When a "pulse" of dry ice was introduced into the air-gun, a sharp vertical front could be observed using strobed lighting which passed through the duct indicating a well-developed turbulent flow, with a uniform air distribution extending to 15.2 cm along the height of the duct and practically all 10.2 cm along the width. A fairly uniform density of dry ice was formed on the leading edge of the sample holder further emphasizing the uniform distribution of material carried by the air flow in the air-gun. Therefore if a sample of less than 15.2 cm height was mounted closed to the exit of the duct and along its axis, the velocity of insects carried by the high velocity stream and impacting the sample would be uniform along the width of the sample.

Using a compressed air supply of 172 kPa in the improved air-gun, an approximate particle velocity of 113 km/hr was visually determined as described in the preliminary study using a polyethylene particle. At 483 kPa, the air velocity within the horizontal cross section of the rectangular duct was determined to be 177 km/hr using a pitot tube. As expected, there was a drop in velocity along the vertical axis of the duct, and almost zero velocity was recorded near the top and bottom of the duct using a pitot tube. After the sample holder was mounted, a small drop in the air velocity directly in front of the sample holder was observed using a pitot tube, when the air valve was fully open (approximately 517 kPa). However, since an insect fed into the feed chute accelerates and reaches the steady state velocity inside the pipe, it was valid to assume that most of its kinetic energy or velocity of the insect was conserved on impact with the target regardless of the drop in the air velocity.

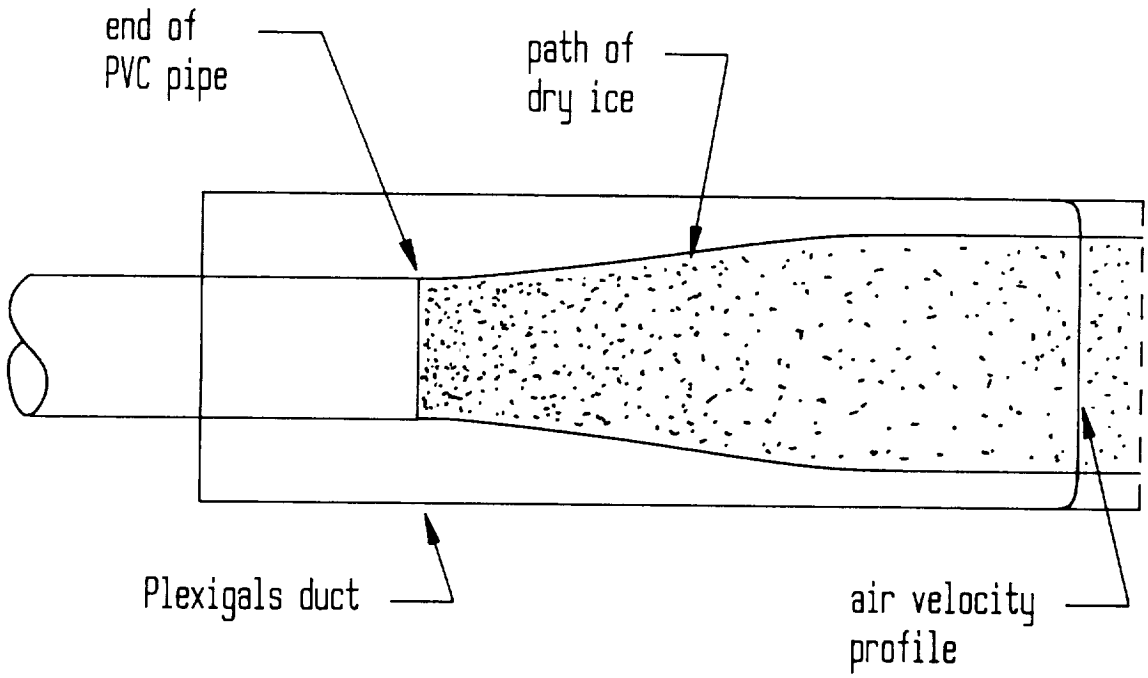

Figure 10: **An profile of the path of dry ice:** The path of dry ice in the plexiglas duct showed that the eddies created by an additional flow of air into the duct had no effect on the air flow exiting from the end of the circular pipe. No flow was seen close to walls of the duct.

3.1.4.5 Insect Impact Using the Air-Gun and Drosophila

FCE-A, B, C and D samples which were prepared as in the phase I and II studies, were tested to compare with the results from the road tests. Other polymer films tested were Teflon^R fluorinated ethylene propylene copolymer (FEP), TEFZEL^R tetrafluoroethylene copolymer, polypropylene, polyethylene, Hostaphan^R polyester, TR-Tedlar^R PVF, plumbing-quality Teflon^R pipe thread tape (Teflon tape), nylon, chlorotetrafluroroethylene (CTFE), polycarbonate, and Teflon^{R}sheet as well as Nyebar^R coating. Thicknesses of these samples are fairly small so that the effect of elasticity of the films on insect adhesion was assumed to be negligible. The surface of Teflon^R sheet was wiped with Kemkit^R wetted with acetone to remove grease from the surface. However, since the preliminary water contact angle measurements on other polymer film surfaces showed only a small variation of contact angles, clean surfaces of the polymer films were assumed and the films were used as received.

Two strips of each polymer film (approximately 1.3×15.2 cm) were glued on a 8.9×35.6 cm aluminum strip, and this aluminum strip was bolted onto the sample holder as shown in Figure 9. This arrangement was similar to the one used in the phase II study, in that the exposed regions of aluminum next to each sample strip were used as control and the normalized percentage (NP) defined in Equation 3.1 was calculated for each sample tested. A minimum of 4 tests (total of 8 strips) per sample were performed.

The polymer film strips were glued onto the aluminum in two different ways -using non-spongy 3M Scotch double-stick tape and spongy 3M Scotch double-sided mounting tape. The samples prepared using non-spongy tape were thin enough that the effect due to the elasticity was assumed to be small, and insect adhesion on the polymer was dominated largely by its surface energy. On the other hand, the spongy tape provides additional elasticity for a given polymer film, so that any difference in the number of insects sticking on the film prepared by these two different ways would be due to the extra elasticity. PVF strips were also glued onto neoprene and Viton^R substrates to obtain intermediate values of elasticity for the tests.

The sample holder carrying sample strips described above was placed in the center of the plexiglas duct as shown in Figure 8, and the air valve fully opened. A large number -approximately 250 or more of Drosophila (fruit flies) were introduced into the air-gun through the feed chute, accelerated to a high velocity and impacted onto the target surface. The number of insects on sample strip and control surfaces for a given polymer film were counted using an optical microscope, and the NP value was calculated.

3.2 Relevant Sample Properties

3.2.1 Surface Analysis

Surface analyses using contact angle measurements, ESCA and SEM were done to characterize the sample elastomers tested in the study, so that the effects of surface properties on insect adhesion could be obtained. Surface analyses were also used to detect visual and quantitative changes of some sample surface due to washing.

3.2.1.1 Contact Angle and Solid Surface Tension Measurements

Contact Angle and Critical Surface Tension When a drop of liquid is placed on a solid, it will either wet the solid or remain as a drop. The liquid drop may have a definite angle between the liquid and solid phase as shown in Figure 11. The angle (θ) is the contact angle and is defined as the angle bewtween a line drawn tangent to the liquid at the liquid/solid contact point and the solid surface. It is important to notice that a non-uniform surface due to surface roughness or surface contamination can change the contact angle. Therefore, much smoother surfaces are required to measure smaller contact angles than larger ones [29].

The contact angle has been used to characterize solid surfaces by many researchers. Zisman [29] has introduced the concept of critical surface energy, γ_c as an empirical method

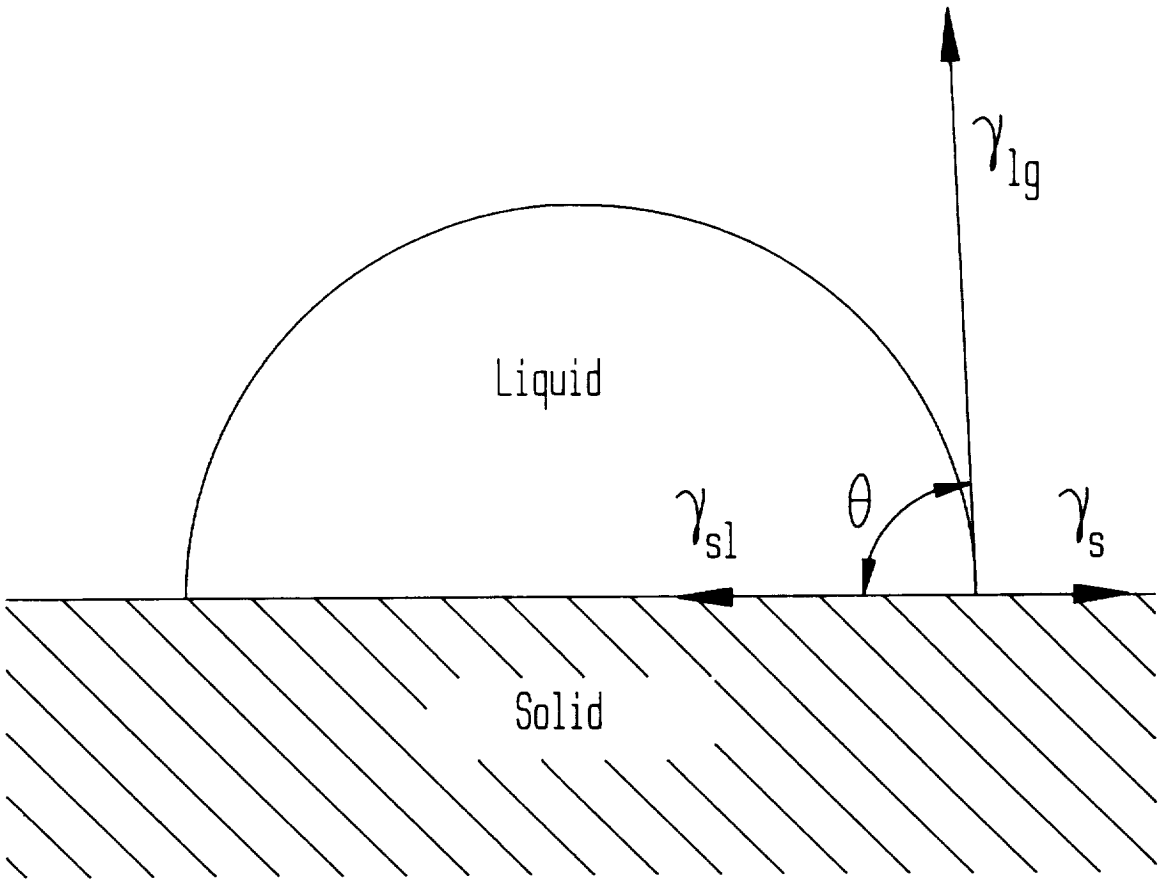

Figure 11: **Contact angle of a sessile drop:** The contact angle (θ) is the angle between a line drawn tangent to the liquid/solid contact point and the solid surface. γ_{sl} is the solid/liquid interfacial surface energy, γ_{lg} is the liquid/vapor interfacial surface energy, and γ_{sg} is the solid/vapor interfacial energy which is usually equal to the solid surface energy (γ_s) [29].

of determining the wettability of solid surface. A plot of $\cos\theta$ versus liquid surface energy (γ_{lg}) for various liquids on a given solid surface is extrapolated to $\cos\theta = 1$, and the corresponding value of liquid surface energy is defined as the critical surface energy of solid, γ_c [29,30]. The critical surface energy, γ_c is the surface energy of the liquid that just wets the solid, so any liquids with γ_{lg} lower than γ_c will spread on the solid surface. The wettability of organic surfaces is commonly determined by the nature and packing of the surface atoms or exposed groups of atoms of the solid, but independent of the nature and arrangements of the underlying atoms and molecules [30].

When $\cos\theta$ is plotted as a function of γ_{lg} for a variety of non-homologous liquids, the points lie close to a straight line or collected around a narrow rectilinear band [29,30]. Certain low surface-energy solids show curvature for values of γ_{lg} above 50 dynes/cm, and this is due to formation of weak hydrogen bonds between the molecules of liquid and molecules in the solid surface. When rectilinear bands are obtained for $\cos\theta$ versus γ_{lg} plots, the intercept of the lower limb of the band at $\cos\theta = 1$ is chosen to be the γ_c [29,30].

Studies show that different values of γ_c for a particular solid surface are obtained depending on the liquid series used in determination. Therefore the liquid series used must be picked with care. Generally, a series of pure liquids are used to determine γ_c, and one series known as the Zisman series are water, glycerol, formamide, methylene iodide and 1-bromonaphthalene. However, a variety of anionic, cation, and nonionic surface active agents and simple organic compounds in aqueous solution [31], mixtures of acetone or ethanol and water [32] are also used to determine γ_c.

Several semiempirical equations have been proposed to determine the solid surface energy (γ_s) and interfacial energy (γ_{sl}). One of them is Owens-Wendt equation that gives the polar and dispersion components of the solid surface energy, and they can be combined to give solid surface energy (γ_s) with reasonable accuracy [33]. The combined Owens-Wendt-Young

equation [34] is given as

$$\frac{\gamma_l(1+\cos\theta)}{2(\gamma_l^d)^{1/2}} = (\gamma_s^d)^{1/2} + (\gamma_s^p)^{1/2}\left(\frac{\gamma_l^p}{\gamma_l^d}\right)^{1/2} \tag{3.5}$$

The subscript l refers to the test liquid and s refers to the solid, and θ is the contact angle for the given liquid on the solid. The superscripts d and p are dispersion and polar components of the surface energy, respectively, and the summation of these values of these two components gives the solid surface energy. When three or more different liquids are tested, the polar and dispersion components of the solid surface energy can be obtained from the slope and intercept of a plot of $\gamma_l\,(1+\cos\theta)/2(\gamma_l^d)^{1/2}$ versus $(\gamma_l^p/\gamma_l^d)^{1/2}$, respectively.

Wetting and Surface Tension Wetting is defined as the displacement from a surface of one fluid by another, and there are three recognized types, namely, spreading, adhesional and immersional wetting [35]. Usually wetting means that the contact angle between a liquid and a solid surface is zero or close to zero such that the liquid easily spreads over the liquid. On the other hand, non-wetting means that the contact angle is greater than 90° so the liquid tends to ball up and run off the surface easily [36]. Since only two types of wetting (spreading and adhesional) are relevant to the present study, these are discussed below.

In spreading wetting, a liquid which is already in contact with the solid surface spreads, so that the solid/liquid and liquid/gas interfacial areas are increased but the solid/gas interfacial area is decreased. The spreading coefficient (S) is defined [36] as

$$S = -\Delta G_s/A = \gamma_{sg} - (\gamma_{sl} + \gamma_{lg}) \tag{3.6}$$

where $-\Delta G_s$ is the free energy due to spreading, γ_{sg} is the surface energy of the solid in equilibrium with the liquid vapor, γ_{lg} is the liquid surface energy, γ_{sl} is the solid/liquid interfacial energy and A is wetting area. γ_{sg} is usually equal to γ_s which is the surface energy of the solid against its own vapor. If S is positive or zero, the liquid will spread spontaneously over the solid surface. If S is negative, the liquid will remain as a drop with

a finite contact angle on the solid surface [35]. Spreading of a particular liquid on a given solid mainly depends of the surface energy of the solid.

The equilibrium contact angle (θ) is determined by a minimum in the total surface free energy, that is the quantity $(-\gamma_{sg}A_{sg}+\gamma_{sl}A_{sl}+\gamma_{lg}A_{lg})$ is a minimum, where A is interfacial area. The change in the free energy of the system by spreading to cover an extra area as shown in Figure 12 is given by

$$dG = \gamma_{sl}dA + \gamma_{lg}dA + \gamma_{sg}dA \tag{3.7}$$

At equilibrium, $dG = 0$ so

$$\gamma_{sl} + \gamma_{lg}\cos\theta - \gamma_{sg} = 0 \tag{3.8}$$

or

$$\cos\theta = (\gamma_{sg} - \gamma_{sl})/\gamma_{lg} \tag{3.9}$$

For a given liquid, if the system is at equilibrium, the contact angle is a function only of $(\gamma_{sg} - \gamma_{sl})$, the surface energy of the solid and the interfacial surface energy.

Adhesional wetting occurs when a liquid which is not originally in contact with the solid surface contacts and adheres to the solid surface. In adhesional wetting, the liquid/gas interfacial area is decreased. The work of adhesion (W_a) is defined [35] as

$$W_a = -\Delta G_a/A = \gamma_{sg} + \gamma_{lg} + \gamma_{sl} \tag{3.10}$$

or

$$W_a = \gamma_{lg}\,(1 + \cos\theta) \tag{3.11}$$

If the contact angle is zero, the solid is completely wetted by the liquid, and only partially wetted if the contact angle is finite.

The wetting of a surface during the impact of insects may be explained by either type of wetting described above. However, with both types of wetting, the contact angle between the liquid and solid surface depends in part on the surface energy of the solid. Increase of the contact angle means that the solid surface becomes more wettable by liquid and the contact area (solid/liquid interfacial area) is increased.

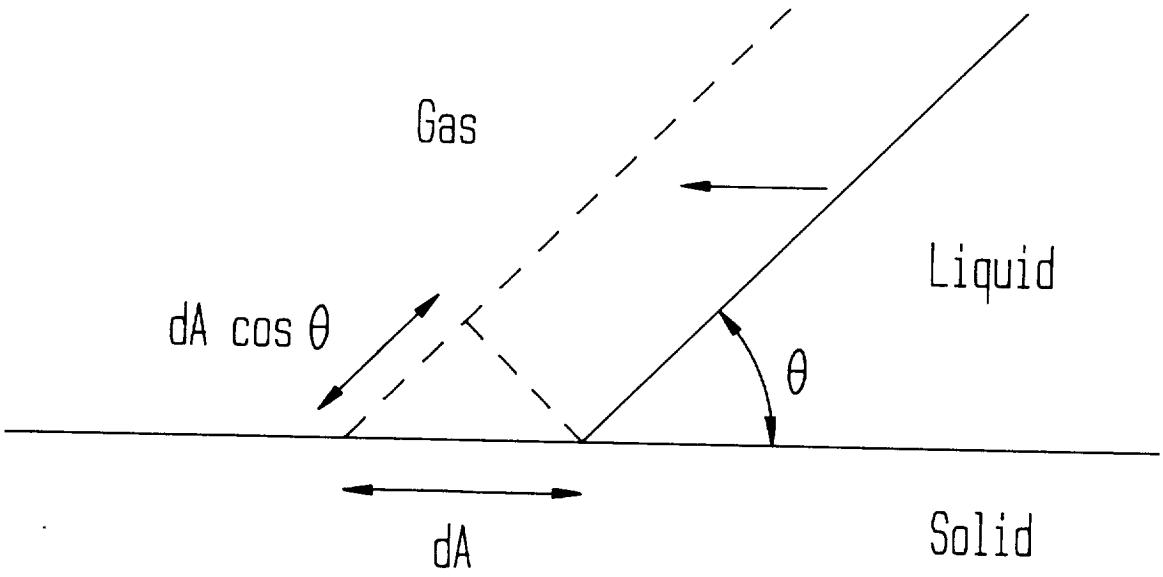

Figure 12: **Illustration of spreading-wetting at equilibrium:** In spreading wetting a liquid surface which is already in contact with the solid surface spreads. θ is the contact angle, and A is the interfacial area [35].

Contact Angle and Solid Surface Tension Measurements The contact angles of all the samples tested were measured with (deionized) water using an NRL contact angle goniometer. In case of the FCE and polyurethane samples, the water contact angles of washed and unwashed samples were measured to detect any changes in the surfaces due to the washing process. Since no information on the roughness or homogeneity of any sample surface were given, a large number of measurements was necessary to reduce errors. Two micro liters (μl) of water were placed on the sample surface and contact angles were measured at both sides. An additional 2 μl was added to the original drop and the advancing contact angles were measured. This procedure was repeated two more times so that the total volume of water on the sample surface was 8 μl. Contact angles of each sample were measured at a minimum of three different locations, and the average contact angle calculated.

The critical surface energies for washed FCE's, neoprene, Viton^{R} and polyurethane were determined using a series of contact angle measurements as described in the previous paragraph with water-to-ethanol solutions. Pure ethanol and deionized water were mixed at six different water to ethanol volume ratios: 100/0, 90/10, 70/30, 50/50, 60/40, 70/30, and 80/20. Also contact angles for all the polymer films tested were measured using pure water, glycerol and formamide. The critical surface energy (γ_c) was obtained from the plot of $\cos\theta$ versus liquid surface energy of water/ethanol solutions. Also a line of $\gamma_l(1+\cos\theta)/2(\gamma_l^d)^{1/2}$ versus $(\gamma_l^p/\gamma_l^d)^{1/2}$ was constructed for both water/ethanol series and water, glycerol and formamide series, and the polar and dispersion solid surface energies of a sample polymer were obtained from the slope and intercept, respectively according to the Owens-Wendt-Young equation given in Equation 3.5. Liquid surface energies and their dispersion and polar components of water/ethanol solutions, pure water, glycerol and foramide are provided in Table II. The water contact angles on the SBR elastomer surfaces were also measured.

3.2.1.2 Scanning Electron Microscopy (SEM)

The SEM image is produced by low energy secondary electrons emitted from the sample as a result of excitation by an incident electron beam [37]. The beam is scanned over any selected area of the sample in a rectangular pattern; the emitted electrons are collected by an electron detector and transformed into an image. SEM images have a wide range of contrast so that detail can be seen both in very dark and in bright areas. Images can also have a great depth of focus; they are very sharp at both low and high points of the surface so even quite rough surfaces show startling clarity and a feeling of depth [36]. SEM is widely used to examine surface topography [36], and resolution down to a few nanometers is possible, depending on the nature of the sample and the type of microscope. SEM photomicrographs can be obtained for most dry solids and bulk material, including inorganic samples, metal, polymeric materials, and biological samples.

SEM was used to study the surface topography of some samples used in this study to observe visually changes in the surface due to the washing process. A disk was punched from each washed and unwashed polyurethane, FCE's, Viton^{R}, and neoprene samples, and sputter coated with gold using an SPI sputter coater for 45 seconds at 35 mA. SEM photomicrographs of both washed and unwashed samples were taken using a JEOL 35C SEM at two different magnifications (x200 and x360) to detect any changes in surface topography.

SEM photomicrographs of Teflon^{R} tape before impact of insects were taken to study the surface topography because of its unusual texuture. The sample disk of Teflon^{R} tape as received without washing the surface was sputter coated with gold using an Edwards S150B sputter coater for 2 minutes at 45 mA. SEM photomicrographs of samples were taken using an ISI SX-40 scanning electron microscope at various magnifications.

Table II: **Dispersion and Polar Components of Liquid Surface Tensions:** These surface tensions and their dispersion and polar components [32] were used to calculate critical surface tensions and solid surface energies for the polymers.

Liquid	γ_l^d (dynec/cm)	γ_l^p (dynes/cm)	γ_l (dynes/cm)
Glycerol	37.0	26.4	63.4
Formamide	39.5	18.4	58.2
Water/Ethanol			
100/0	22.0	50.2	72.2
90/10	19.9	31.3	51.2
70/30	17.3	17.6	34.9
50/50	19.2	12.3	31.5
40/60	18.9	10.4	29.3
70/30	19.4	9.7	29.1
80/20	18.6	8.3	26.9

3.2.1.3 Electron Spectroscopy for Chemical Analysis (ESCA)

X-ray photoelectron spectroscopy (XPS) or electron spectroscopy for chemical analysis (ESCA) was originated by Professor Siegbahn at Uppsala University in Sweden [37]. In ESCA a sample is irradiated with an incident beam of x-rays in a ultra-high vacuum [38]. When the x-ray energy ($h\nu$) exceeds the binding energy of the electron (E_b), absorption of x-ray photons by atoms in the sample causes electrons to be ejected. Photoemitted electrons leave the sample with kinectic energy E_k, that is measured by the ESCA spectrometer [37]. This process can be described by the following energy conservation equation[39]:

$$h\,\nu = E_k + E_b + \phi_s \tag{3.12}$$

Since the E_b is a characteristic of the atomic orbital and ϕ is a charging correction, an element present on the sample surface can be identified from the ESCA spectra.

Small changes in binding energies of atomic orbitals give rise to what is called the "chemical shift effect" in ESCA [38]. For example, changes which generate a lower electron density at the nucleus of an atom tend to increase slightly the binding energies of the atomic orbitals. Thus, these chemical shifts can reveal the oxidation state of an element or its presence in a particular functional group or chemical environment such as nitrogen in amines, ammonium ions, nitrites or nitrates [40].

ESCA is a surface-analysis technique for a wide range of samples, including organic and inorganic materials, such that oxidation state, organic structure and bonding information can be obtained. Although ESCA can detect all elements except hydrogen, its vacuum requirements for analysis limit samples to solid materials. Quantitative analysis is feasible for films and other smooth surfaces, but is difficult for powders [37].

Some of its applications are listed as follow:

- Determination of the surface composition of multicomponent polymer films [41].

- Determination of oxidation state changes at the surface of a sample [39,42]
- Investigation of surface contamination problems for both organic and inorganic materials [41,43].
- Surface adsorption studies for the case which adsorbed species is bonded strongly enough to resist the vacuum necessary for analysis [37].
- Studies of catalysts, including oxidation state determinations and surface enrichment effect, leading to structure-activity correlations and identification of changes upon aging [37,39].

Unwashed and washed polyurethane, FCE-A, B, and C samples were analyzed quantitatively using ESCA. ESCA spectra are obtained at a 90 °take-off angle using a Kratos XSAM 800 spectrometer with a Mg-K_α x-ray source. Comparison of these ESCA results lead to a clearer understanding of the observed changes in the contact angles due to washing these samples. All other samples used in this study were similarly analyzed quantitatively using ESCA to detect the elements present on their surfaces.

3.2.2 Modulus of Elasticity

A material is called elastic when the deformation produced in the body is completely recovered after the applied force is removed. The modulus of elasticity in tension, or Young's modulus (E) is [45]

$$\mathrm{E} = \sigma/\tau \tag{3.13}$$

where σ is the tensile stress which is the normal force acting per unit area of a plane, and τ is the tensile strain or deformation which is the elongation per unit length [45]. A better elastomer will have a higher deformation or a smaller modulus.

Dog-bone specimens were cut from the elastomer samples, and neck lengths and thickness were measured. The dog-bones were stretched in an Instron tensile test at a cross-head

speed of 10.0 mm/min until a plot of load (kg) versus elongation (mm) was achieved. A modulus of elasticity (E) for a given sample was calculated from a plot obtained on the Instron using the equation:

$$E = \frac{\text{slope of the plot} \times g \times \text{length of neck}}{\text{area} \times C} \tag{3.14}$$

The elongation obtained from the slope of the plot is corrected to the actual elongation using a correction factor – crossed speed divided by chart speed. The area in Equation 3.14 is calculated as the product of thickness and width of the neck of the dog-bone; g is the acceleration of gravity, C is a conversion factor (1 $kg\,m/s^2/N$, or 32.174 $lb_m\,ft/s^2/lb_f$).

Chapter 4

Results and Discussion

4.1 Surface Analysis Results

SEM, ESCA and contact angle measurements using a goniometer have proved to be useful techniques in detecting changes on the polymer surfaces due to washing, determination on surface energy, and measurements of surface compositions for all polymers studied.

4.1.1 Detecting Changes on Surfaces Using Surface Analysis

The presence of contaminants on the elastomers used in the phase I study was examined by analyzing surfaces of both washed and unwashed samples. Samples were washed using a commercial detergent (Tide^{R}) in water. Any changes due to washing are easily detected from water contact angle measurements of washed and unwashed FCE's and polyurethane samples, and these results are provided in Table III. Standard deviations calculated for unwashed samples are higher than those for washed samples. These larger variations in water contact angle measurements on the unwashed samples are due to the presence of contamination. The contact angles for washed FCE samples are much higher than for

Table III: **Average Water Contact Angles of Washed and Unwashed Fluorocarbon Elastomers (FCE) and Polyurethane (PU)**

Sample	Unwashed (degrees)	Washed (degrees)
FCE–A	77±6	92±2
FCE–B	76±4	94±1
FEC–C	80±5	93±1
FCE–D	83±4	96±1
FCE–E	80±3	96±1
PU	80±4	70±2

unwashed ones, while a lower angle resulted for the polyurethane after washing. The reason for these trends will be explained later using surface-composition results obtained from ESCA analysis.

SEM photomicrographs given in Figure 13, clearly illustrate differences in elastomer surfaces before and after washing. SEM photomicrographs of the unwashed samples show non-homogeneous surfaces with large numbers of holes or irregular patterns. In contrast, the photomicrographs of washed samples show homogeneous and smooth surfaces with small numbers of holes or irregular patterns. Thus, the washing and rinsing process have removed the non-homogeneous top layer (probably contaminants) of the unwashed sample, and left an apparently clean surface. So the lower contact angles for the unwashed surfaces might be caused by a covering layer on the surface. SEM photomicrographs of the polyurethane sample show minimal changes. However, the average contact angle of washed polyurethane is lower than for the unwashed one. No clear cause for this may be concluded from the SEM photomicrographs.

SEM photomicrographs of stretched and unstretched Teflon^{R} tape are shown in Figure 14. The photomicrographs of unstretched tape surface show spots (islands) which are smooth and homogeneous with no holes. These spots are connected by ridges which are parallel to each others and form different sized gaps. These ridges have been deformed by stress applied normal to them as shown in photomicrographs of stretched tape in Figre 14. However, tests using the air-gun show that alteration in this surface structure appears to have littlte effect on the number of insects sticking onto the Teflon^{R} tape.

Comparison of ESCA results of selected samples lead to a clearer understanding of the observed changes in the contact angles and differences in the SEM photomicrographs due to washing. As shown in Tables IV and V, some of elements detected on the unwashed samples are not present on the washed samples. The atomic percent ratios given in Table V are calculated by comparing the atomic composition of each element to the value for carbon. For most samples, washing has removed some or all of the contamination on the unwashed

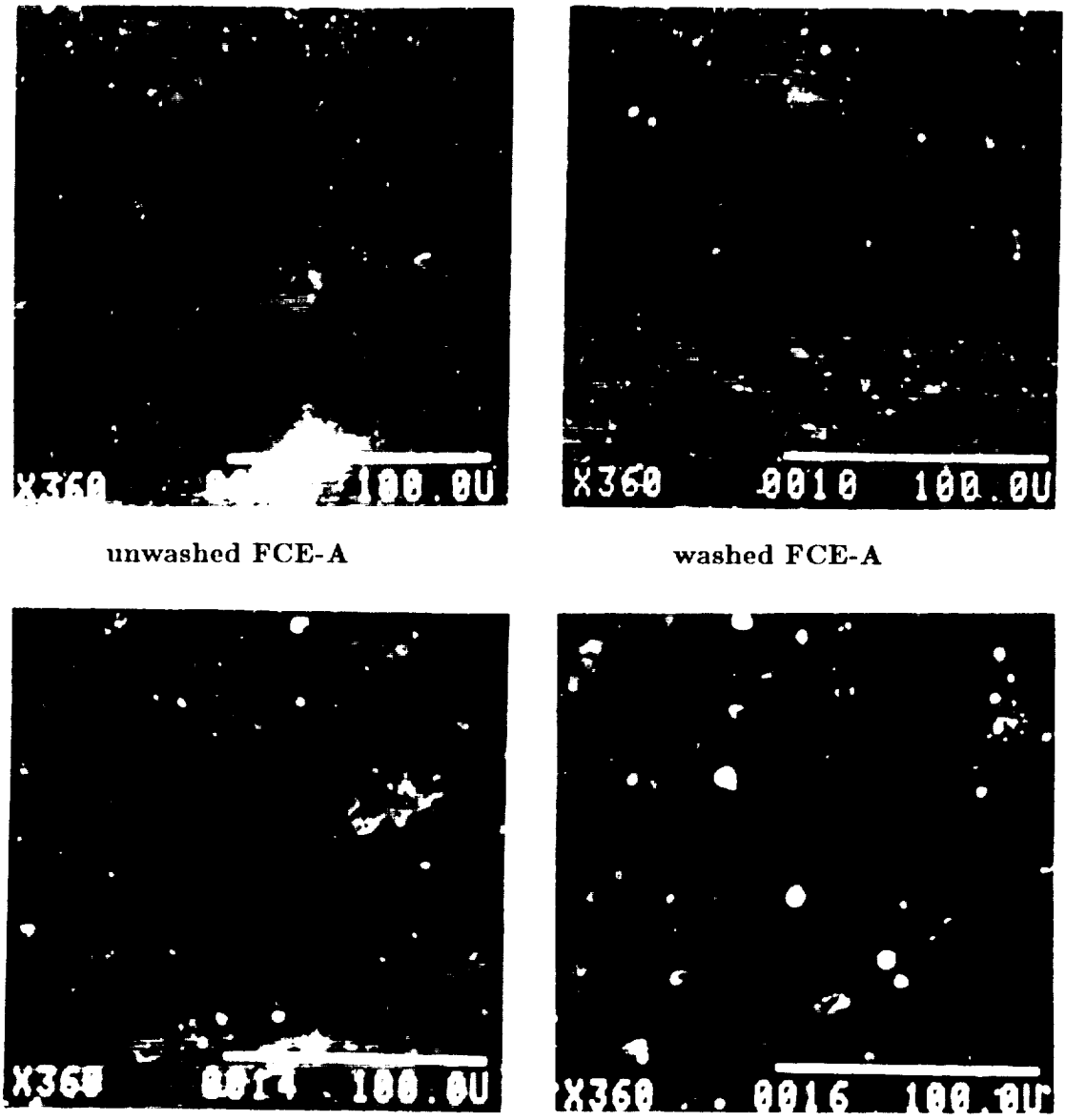

unwashed FCE-A

washed FCE-A

unwashed FCE-B

washed FCE-B

Figure 13: **SEM photomicrographs of washed and unwashed elastomers:** There are a large number of holes or irregular patterns on unwashed samples, but smooth surfaces with a small number of holes or irregular patterns are seen in the photomicrographs of washed elastomers.

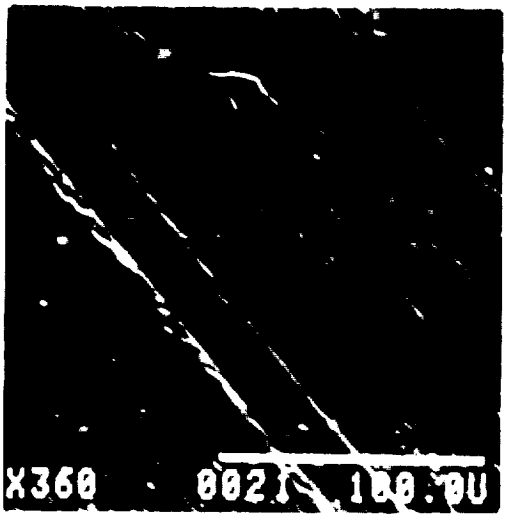

unwashed FCE-C

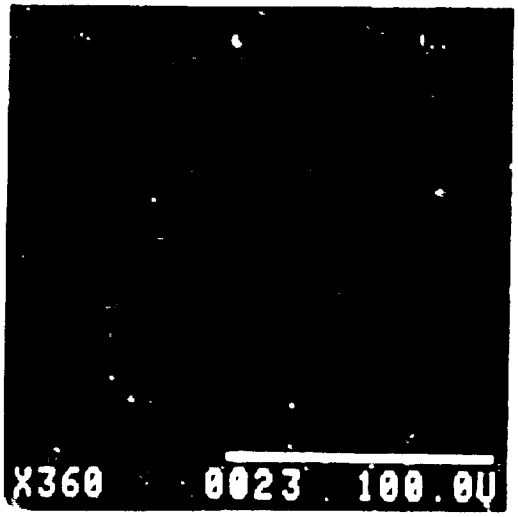

washed FCE-C

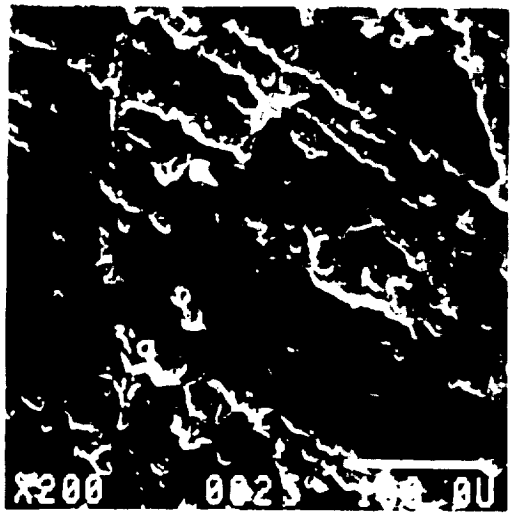

unwashed FCE-D

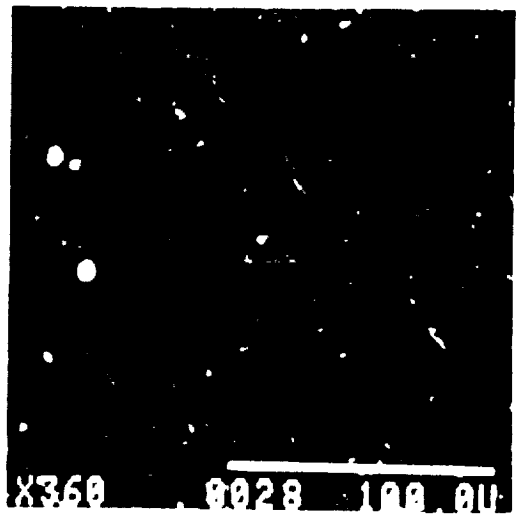

washed FCE-D

Figure 13 continued.

unwashed FCE-E

washed FCE-E

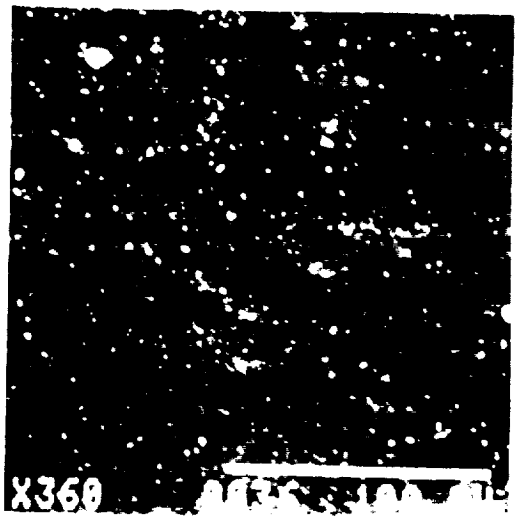

unwashed neoprene

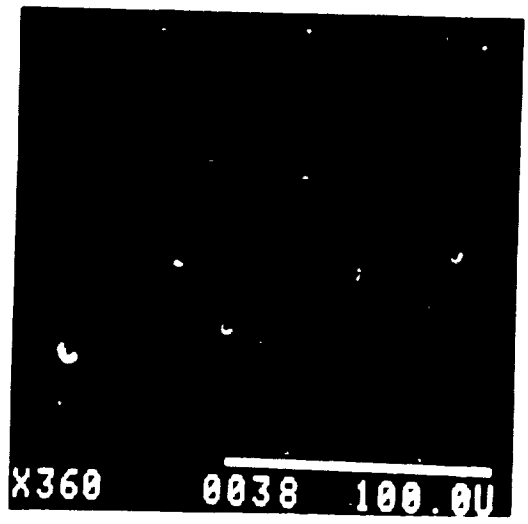

washed neoprene

Figure 13 continued.

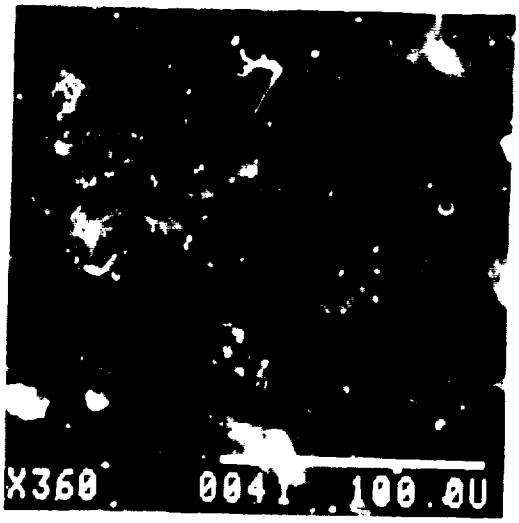

unwashed Viton^{R}

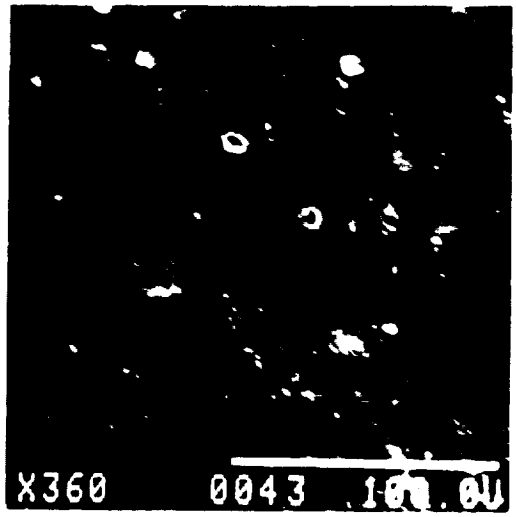

washed Viton^{R}

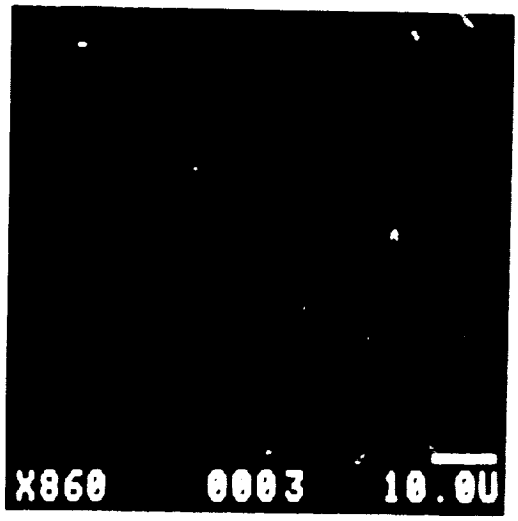

unwashed polyurethane

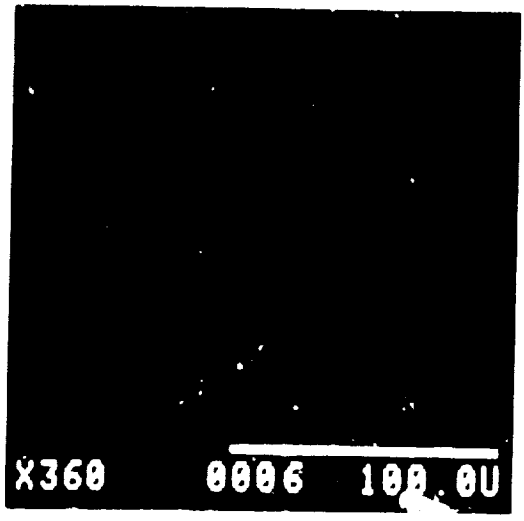

washed polyurethane

Figure 13 continued.

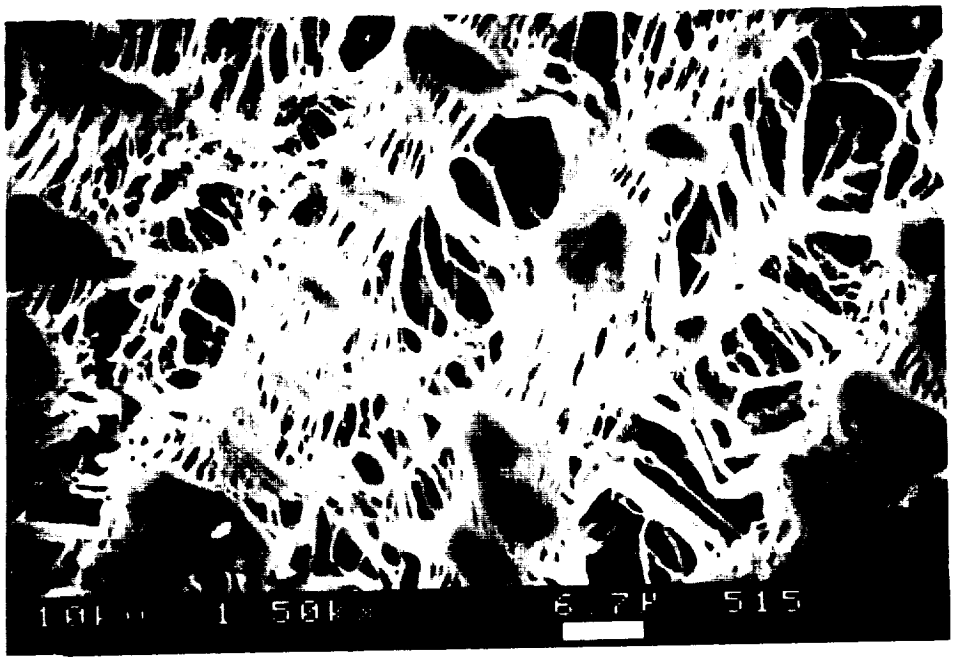

unstretched Teflon^R tape

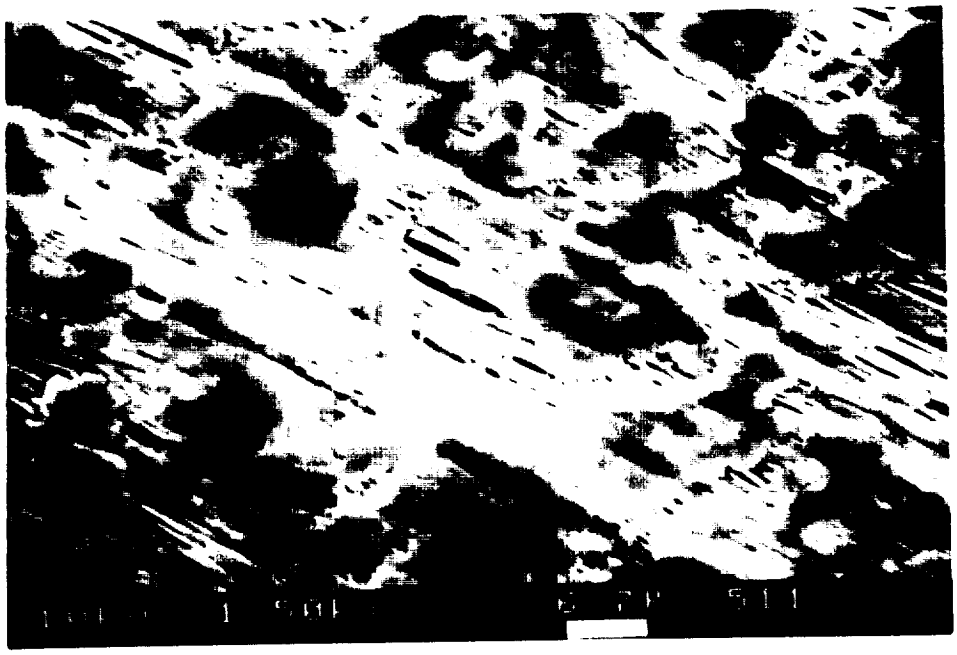

stretched Teflon^R tape

Figure 14: SEM photomicrographs of stretched and unstretched Teflon^R tape:

sample surfaces due to elements such as nitrogen, calcium, sulfur and silicon. The presence of such contamination altered water contact angles for the unwashed sample surfaces. Also, it may be concluded that these elements formed the non-homogeneous top layer shown in the SEM photomicrographs, but which is removed by washing. ESCA analyses of the unwashed and washed FCE elastomers show a large increase of the fluorine content on the surfaces of the washed samples. Since the surface contaminants are removed by washing, the highly fluorinated surfaces of the FCE samples become exposed.

The reason for changes in the contact angles of the washed samples may be explained by comparison of the fluorine composition obtained from ESCA spectra. The fluorine composition on a polymer surface has an important effect on the contact angle; the surface with a higher fluorine composition has a lower surface energy, and hence a higher contact angle results. The calculated atomic fraction of fluorine on the washed FCE surfaces is higher than on unwashed ones, so that higher contact angles are observed for the washed surfaces. The polyurethane sample shows the opposite result from FCE samples; a very small amount of fluorine (0.7%) has been removed from the surface after washing, which results in a lower contact angle after washing.

4.1.2 Contact Angle and Critical Surface Tension Measurements

Contact angle measurements using water/ethanol solutions with different volume ratios for FCE's, neoprene, Viton^{R}, and polyurethane sample elastomers are summarized in Table VI. At any water/ethanol volume ratios, contact angles for neoprene and Viton^{R} are higher than any other samples, while the lowest contact angles are obtained with the polyurethane sample. These measurements yield an extrapolated critical surface energy of about 25 dynes/cm for all samples shown in Figure 15 and Table VII. This unexpected constant value is close to the surface energy of pure ethanol. These results are similar to those obtained by Dann [32], when critical surface energies of various polymers were close to 25 dynes/cm as shown in Table VIII. Although no definite conclusion can be drawn at present, one possibility that

Table IV: **ESCA Atomic Composition (%) of Washed and Unwashed Elastomer Samples.**

Sample	Photopeak						
	C1s	O1s	F1s	Si2p	N1s	Ca2p	S2p
Unwashed FCE–A	78.0	8.5	8.8	2.8	1.5	0.6	0.2
Washed FCE–A	63.0	3.2	33.0	0.5	—	—	—
Unwashed FCE–B	72.0	9.0	14.0	2.7	1.3	0.5	—
Washed FCE–B	64.0	6.7	28.0	1.9	—	—	—
Unwashed FCE–C	73.0	9.1	12.0	3.4	1.6	0.4	—
Washed FCE–C	60.0	4.0	36.0	0.2	0.2	—	—
Unwashed PU	82.0	13.0	0.7	1.7	0.8	1.5	—
Washed PU	81.0	16.0	—	0.4	2.4	—	—

Table V: **ESCA Atomic Ratios of Washed and Unwashed Elastomer Samples.**

Sample	Ratio					
	O/C	F/C	Si/C	N/C	Ca/C	S/C
Unwashed FCE–A	0.110	0.110	0.036	0.019	0.008	0.003
Washed FCE–A	0.051	0.520	0.008	—	—	—
Unwashed FCE–B	0.120	0.190	0.038	0.018	0.007	—
Washed FCE–B	0.100	0.440	0.030	—	—	—
Unwashed FCE–C	0.120	0.160	0.046	0.022	0.005	—
Washed FCE–C	0.067	0.600	0.003	0.003	—	—
Unwashed PU	0.160	0.009	0.021	0.010	0.018	—
Washed PU	0.200	—	0.005	0.030	—	—

may account for this result is that ethanol preferentially adsorbs on the low energy polymer surfaces, and invalidates the use of water/ethanol solutions to measure γ_c.

As an alternate approach, solid surface energies may be calculated using the Owens-Wendt-Young equation given in Equation 3.5. This equation predicts that a plot of $\gamma_l(1+\cos\theta)/2(\gamma_l^d)^{1/2}$ versus $(\gamma_l^p/\gamma_l^d)^{1/2}$ will be a straight line. Dispersion and polar solid surface energies are obtained from the intercept $((\gamma_s^d)^{1/2})$ and slope $((\gamma_s^p)^{1/2})$, respectively. The solid surface energies of FCE's, neoprene,Viton^{R}and polyurethane were calculated from the sum of dispersion and polar surface energies, which were obtained by fitting the experimental data to the Owens-Wendt-Young equation, using linear regression. Since adsorption of ethanol onto the sample surface is expected as described in the previous paragraph, only the four highest contact angles of water/ethanol solutions were used.

As shown in Table IX, the surface energies of the FCE samples are approximately the same as the surface energies of the Viton^R and neoprene. However, these results are unexpected since the contact angles of these last two samples are larger than for the FCE samples for any of the water/ethanol volume ratios, as shown in Table VI. This might be due to the small differences in measured contact angles between Viton^R, neoprene and FCE samples. These small differences become insignificant in the calculation of $\gamma_l(1+cos\theta)/2(\gamma_l^d)^{1/2}$ which implies that water/ethanol mixtures might be inappropriate to use with the Owens-Wendt-Young equation for discriminating small differences in solid surface energies. However,the surface energy for polyurethane is calculated to be 32 dynes/cm, higher than any other elastomers. This higher value for polyurethane is expected since contact angles obtained with any water/ethanol volume ratio are much lower than for the other samples as shown in Table VI. Thus the results of the surface energies obtained from the Owens-Wendt-Young equation are somewhat more reliable than those obtained from extrapolated critical surface energies.

Contact angle measurements using water, glycerol, and formamide for the polymer films are provided in Table X. The solid surface energies together with their polar and disper-

Table VI: **Contact Angle Measurements With Water/Ethanol Solutions at Different Volume Ratios.**

Sample	Water/Ethanol (ml/ml)						
	100/0	90/10	70/30	50/50	40/60	30/70	20/80
FCE-A	92±2	85±2	66±2	50±2	48±1	40±1	25±3
FCE-B	94±1	84±3	69±2	53±2	46±3	39±1	28±2
FCE-C	93±1	83±3	67±3	51±3	48±2	36±2	spreads
FCE-D	96±1	84±3	65±2	47±2	46±2	34±2	23±3
FCE-E	96±1	84±3	67±2	50±1	38±1	31±1	spreads
PU	70±2	60±2	48±2	28±3	23±2	spreads	spreads
Neoprene	102±1	93±2	75±2	61±2	57±2	44±1	39±1
Viton^R	103±2	95±2	76±2	66±2	55±2	40±1	39±1

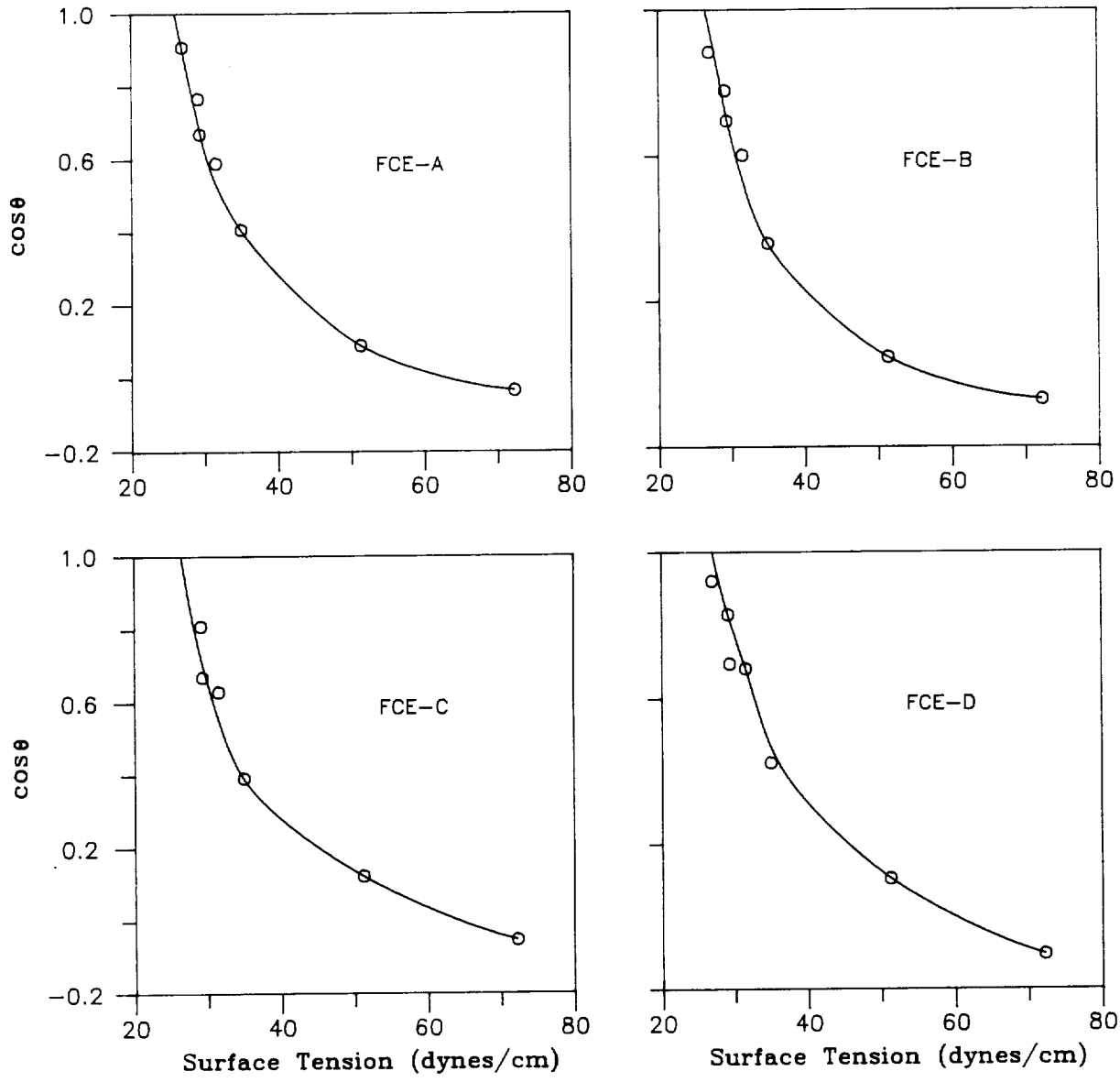

Figure 15: **cos θ versus surface energy of water/ethanol solution:** The plots of cos θ vs. surface energy of water/ethanol solution at different volume ratios for elastomers are constructed to obtain the critical surface energies (γ_c). γ_c is the surface energy at cos $\theta = 1$.

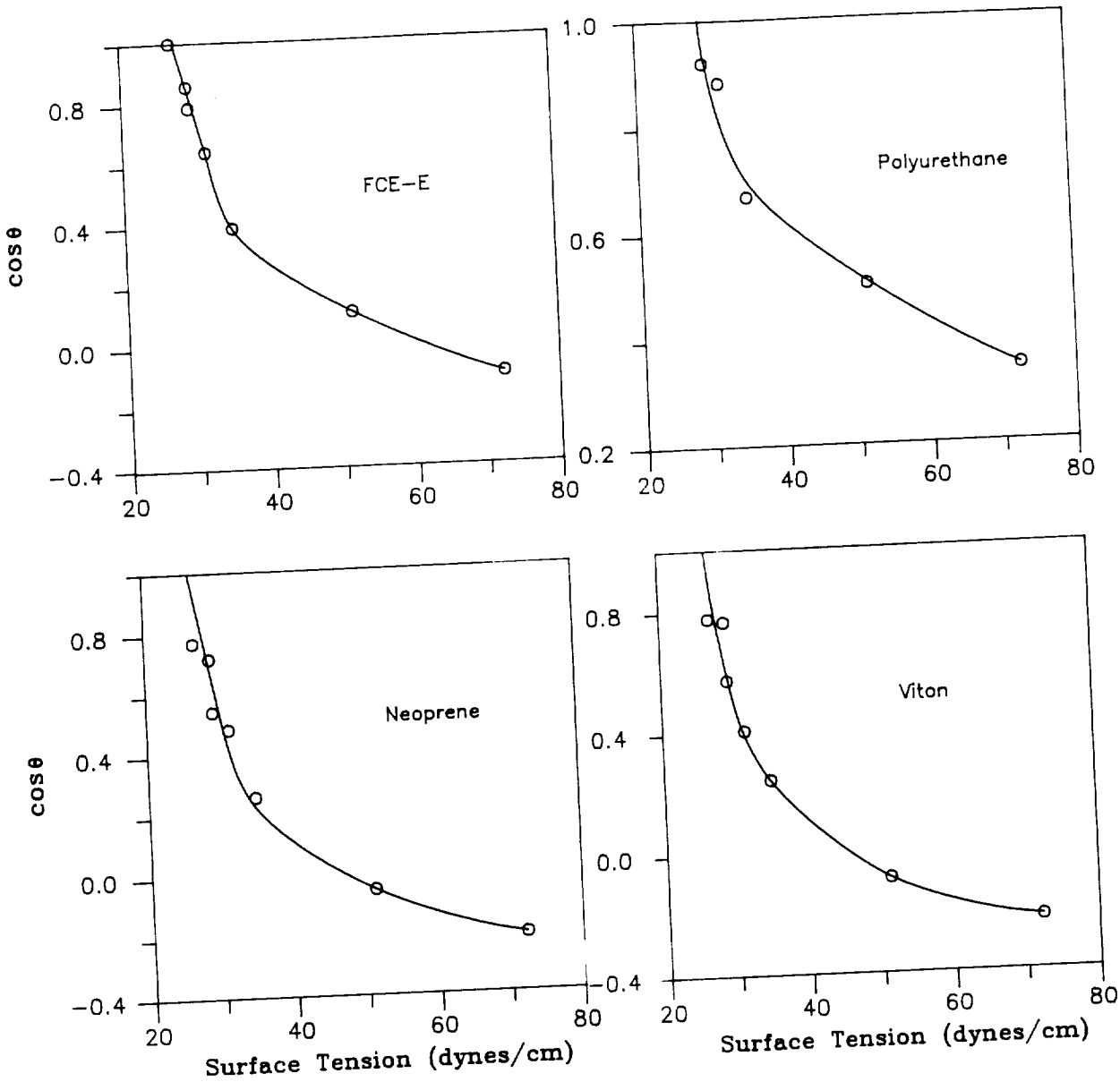

Figure 15 continued.

Table VII: **Extrapolated Critical Surface Tensions (γ_c) Obtained from Plots of $\cos\theta$ versus Liquid Surface Tension Using Water/Ethanol Solutions at Different Volume Ratios.**

Sample	γ_c (dynes/cm)
FCE–A	26
FCE–B	27
FCE–C	27
FCE–D	27
FCE–E	28
PU	29
Neoprene	27
Viton^R	27

Table VIII: **Critical Surface Tensions (γ_c) of Various Polymers Using Water/Ethanol Solutions According to Dann.**

Polymer	γ_c^1 (dynes/cm)
Teflon	19.0
Polyethylene	25.5
Polystyrene	27.0
Polyvinyl chloride	26.0
Polymethyl methacrylate	26.5
Polyethylene terephthalate	27.0
Nylon 11	26.0
Nylon 6,6	28.0

1. Reference [32].

Table IX: **Critical Surface Tensions (γ_s) of the Elastomers Obtained from Plots Using the Owens-Wendt-Young Equation.**

Elastomer	γ_s (dynes/cm)	Correlation Coefficient (r)
FCE–A	21	0.9172
FCE–B	19	0.9282
FCE–C	21	0.9743
FCE–D	25	0.9164
FCE–E	23	0.9164
PU	32	0.9725
Neoprene	20	0.8550
Viton^R	20	0.7663

sion components, obtained from slopes and intercepts by fitting the experimental data to the Owens-Wendt-Young equation using linear regression, are given in Table XI. A wide range of polymer surface energies are obtained from the lowest value of 5 dynes/cm for the teflon tape to the highest value of 44 dynes/cm for the PVF, which are expected from the contact angle measurements with water, glycerol and formamide. Correlation coefficients calculated for any polymer sample (except Teflon^R tape) are better than those calculated for water/ethanol solution series given in Table VII.

As shown in Table X, a wide range of water contact angles for sample surfaces are obtained. The samples with larger contact angles are expected to have lower surface energies than those with smaller contact angles. The surface energies obtained from plots of the Owens-Wendt-Young equation for FCE elastomers show no significant differences in their values, while little differences in water contact angles are observed for these sample elastomers. Thus, the water contact angles for a given set of samples, which are easily measured without having to make a large number of contact angle measurements with various liquids, can indicate a relative ordering of surface energies for the samples. Since the contact angle is inversely related to the surface energy, any sample with a high water contact angle has a low surface energy. For example, the Teflon^R tape which exhibits the largest water contact angle of 121° is expected to have the lowest surface energy, while the highest surface energy for the PVF sample with a water contact angle of 60° is expected. As predicted from the water contact angle measurements, the lowest value of 5 dyne/cm and the highest value of 44 dyne/cm for the Teflon^R tape and PVF, respectively, are obtained using the Owens-Wendt-Young equation as described previously.

4.1.3 Determination of Surface Composition

The calculated elemental atomic compositions and ratios for FCE's, polyurethane, neoprene and Viton^R elastomers are listed in Tables XII and XIII. Bulk fluorine concentrations of FCE-A and B are reported to be the same (69%) while FCE-C, D and E are reported

Table X: **Contact Angles of Water, Glycerol and Formamide on Polymer Films.**

Polymer Film	Contact Angle (degrees)		
	Water	Glycerol	Formamide
Polypropylene	101 ± 3	90 ± 2	83 ± 2
Polyester	65 ± 2	62 ± 1	58 ± 2
CTFE	92 ± 2	82 ± 2	73 ± 2
Polycarbide	77 ± 1	67 ± 1	56 ± 1
Polyethylene	95 ± 2	86 ± 2	82 ± 1
Nybar^R	109 ± 3	—	—
PVF	60 ± 2	54 ± 2	37 ± 2
TEFZEL	95 ± 2	85 ± 2	76 ± 2
FEP	108 ± 1	99 ± 1	90 ± 1
Teflon^R Sheet	108 ± 2	104 ± 1	91 ± 1
Tefon^R Tape	121 ± 1	123 ± 2	108 ± 3

Table XI: **Surface Energies (γ_s) and Their Polar (γ_s^p) and Dispersion (γ_s^d) Components of Polymer Films.**

Sample	γ_s^d (dynes/cm)	γ_s^p (dynes/cm)	γ_s (dynes/cm)	Correlation Coefficient
Polypropylene	12.5	4.9	17.4	0.9888
Polyethylene	1.2	21.0	22.2	0.9897
Polyester	22.3	14.2	36.5	0.9995
PVC	19.1	16.3	35.4	0.9981
PVF	17.6	26.3	43.9	0.9839
TEFZEL	3.1	19.2	22.1	0.9748
FEP	0.8	14.5	15.3	0.9087
CTFE	3.5	20.6	24.1	0.9772
Polycarbonate	25.2	8.5	33.7	0.9862
Teflon^R Sheet	12.4	0.1	12.5	0.9337
Teflon^R Tape	1.3	3.7	5.0	0.7226

to be somewhat lower (66%) by the manufacturer (3M). However, the surface fluorine concentrations of FCE's calculated from the ESCA spectra differ from the bulk composition, but differences in chemical composition between the bulk and the surface of a polymer are well documented. The polymer films tested in the air-gun are grouped according to the elemental atomic fraction obtained from the ESCA spectra. As shown in Tables XIV and XV the polymer films are separated into two groups: fluorinated and nonfluorinated polymers, and the relationship between the surface energy of these samples and the number of insects sticking is examined separately.

Table XII: **ESCA Atomic Composition Determined on Elastomer Samples.**

Sample	Photopeak						
	C1s	O1s	F1s	Si2p	N1s	Cl2p	Pb4f
FCE–A	53.0	3.2	33.0	0.5	—	—	—
FCE–B	64.0	6.7	28.0	1.9	—	—	—
FCE–C	60.0	4.0	36.0	0.2	0.2	—	—
FCE–D	59.0	4.3	36.0	0.3	—	—	—
FCE–E	60.0	5.4	34.0	0.7	—	—	—
PU	81.0	16.0	—	0.4	2.4	—	—
Neoprene	62.0	20.0	—	18.0	—	1.1	—
Viton^{R}	46.0	23.0	12.0	18.0	0.5	—	1.0

Table XIII: **ESCA Atomic Ratios of Elastomer Samples.**

Sample	Ratio					
	0/C	F/C	Si/C	N/C	Cl/C	Pb/C
FCE–A	0.060	0.620	0.009	—	—	—
FCE–B	0.100	0.440	0.030	—	—	—
FCE–C	0.0672	0.600	0.003	0.003	—	—
FCE–D	0.073	0.610	0.005	—	—	—
FCE–E	0.090	0.570	0.012	—	—	—
PU	0.200	—	0.005	0.030	—	—
Neoprene	0.320	—	0.290	—	0.018	—
Viton^{R}	0.500	0.260	0.390	0.011	—	0.022

Table XIV: **ESCA Atomic Composition Determined on Polymer Films.**

Polymer		Photopeak						
		C1s	O1s	N1s	Na1s	Cl1s	F1s	Si1s
Nonfluorinated	Polyethylene	99.4	0.6	—	—	—	—	—
	Polypropylene	92.3	5.0	2.7	—	—	—	—
	Polyester	72.4	27.6	—	—	—	—	—
	Polycarbonate	79.8	18.1	—	1.5	0.6	—	—
Fluorinated	PVF	72.0	8.5	—	—	—	19.5	—
	CTFE	51.8	2.1	—	—	10.5	34.3	1.3
	FEP	31.3	0.3	—	—	—	68.6	—
	TEFZEL	32.5	0.6	—	—	—	66.9	—
	Teflon^R	37.2	0.5	—	—	—	62.3	—
	Teflon^R Tape	33.5	0.6	—	—	—	65.9	—

4.2 Insect Impact Studies

The effects of elasticity and surface energy of polymers coated on aluminum on reducing the insect sticking problem are examined. As described in Chapter 3, the normalized percentage (NP) for each sample is calculated and compared instead of the absolute number of insects on different samples. Thus, a sample with a larger NP value has a greater number of insects sticking onto its surface than one with a lower NP value.

4.2.1 Insect Flux Across the Half-Cylinder

The uniformity of the insect flux across the half-cylinder was examined in the road test using aluminum strips as described in Chapter 3. The results from the three road tests performed to study the insect distribution across the half-cylinder are given in Table XVI. The deviation (in percent) for each strip from the average number of insects collected during each road test and all three road tests is calculated using the following equation.

$$\mathrm{PD} = \frac{N_i - N_{al}}{N_i} \times 100 \tag{4.1}$$

where PD is the average deviation (in percent), N_i is the average number of insects for one strip based on the total number of insects sticking on all sample strips, and N_{al} is the number of insects sticking to an aluminum strip. The value of N_{al} in turn is given by the total number of insects on all aluminum strips divided by the number of aluminum strips. As shown in Figure 16, a nonuniform insect distribution or flux across the half-cylinder resulted in each of three tests. Smaller deviations are observed for most strips if the combination of all three tests are considered instead of each individual test. However, a deviation of $\pm$ 20% is still too large to assume a uniform insect distribution across the half-cylinder in the road test even if the average of three road tests per sample is used.

Thus, all three road tests show a nonuniform insect density distribution across the half-cylinder presumably due to a variable insect flux. This variable insect flux probably introduced significant experimental error in the results obtained during road tests in the phase

Table XV: **ESCA Atomic Ratio Determined on Polymer Films.**

Polymer		Photopeak					
		O/C	N/C	Na/C	Cl/C	F/C	Si/C
Nonfluorinated	Polyethylene	0.006	—	—	—	—	—
	Polypropylene	0.054	0.029	—	—	—	—
	Polyester	0.381	—	—	—	—	—
	Polycarbonate	0.227	—	0.019	0.008	—	—
Fluorinated	PVF	0.118	—	—	—	0.271	—
	CTFE	0.041	—	—	0.203	0.662	0.026
	FEP	0.010	—	—	—	2.192	—
	TEFZEL	0.018	—	—	—	2.058	—
	Teflon^{R}	0.013	—	—	—	1.675	—
	Teflon^{R}Tape	0.018	—	—	—	1.967	—

Table XVI: **Insect Distribution Across the Half-Cylinder Using Aluminum Strips.**

Postion of Aluminum Strips from Left Edge of the Half-Cylinder	Number of Insects			
	May 28	July 4	July 20	Total
1	6	17	51	74
2	9	25	49	83
3	5	12	45	62
4	3	9	64	76
5	5	17	42	64
6	2	29	46	77
7	6	21	46	73
8	3	19	35	57
9	4	23	43	70
10	3	23	38	64
11	7	23	39	69
12	6	17	56	79

Table XVI continued

Postion of Aluminum Strips from Left Edge of the Half-Cylinder	Number of Insects			
	May 28	July 4	July 20	Total
13	8	28	47	83
14	6	18	50	74
15	6	18	55	79
16	6	14	50	70
17	10	13	45	68
18	7	27	42	77
19	8	22	46	78
20	7	18	44	69
21	6	15	43	64
22	4	17	43	64
23	4	25	38	67
24	4	19	43	88
25	4	15	52	71
26	3	12	44	59

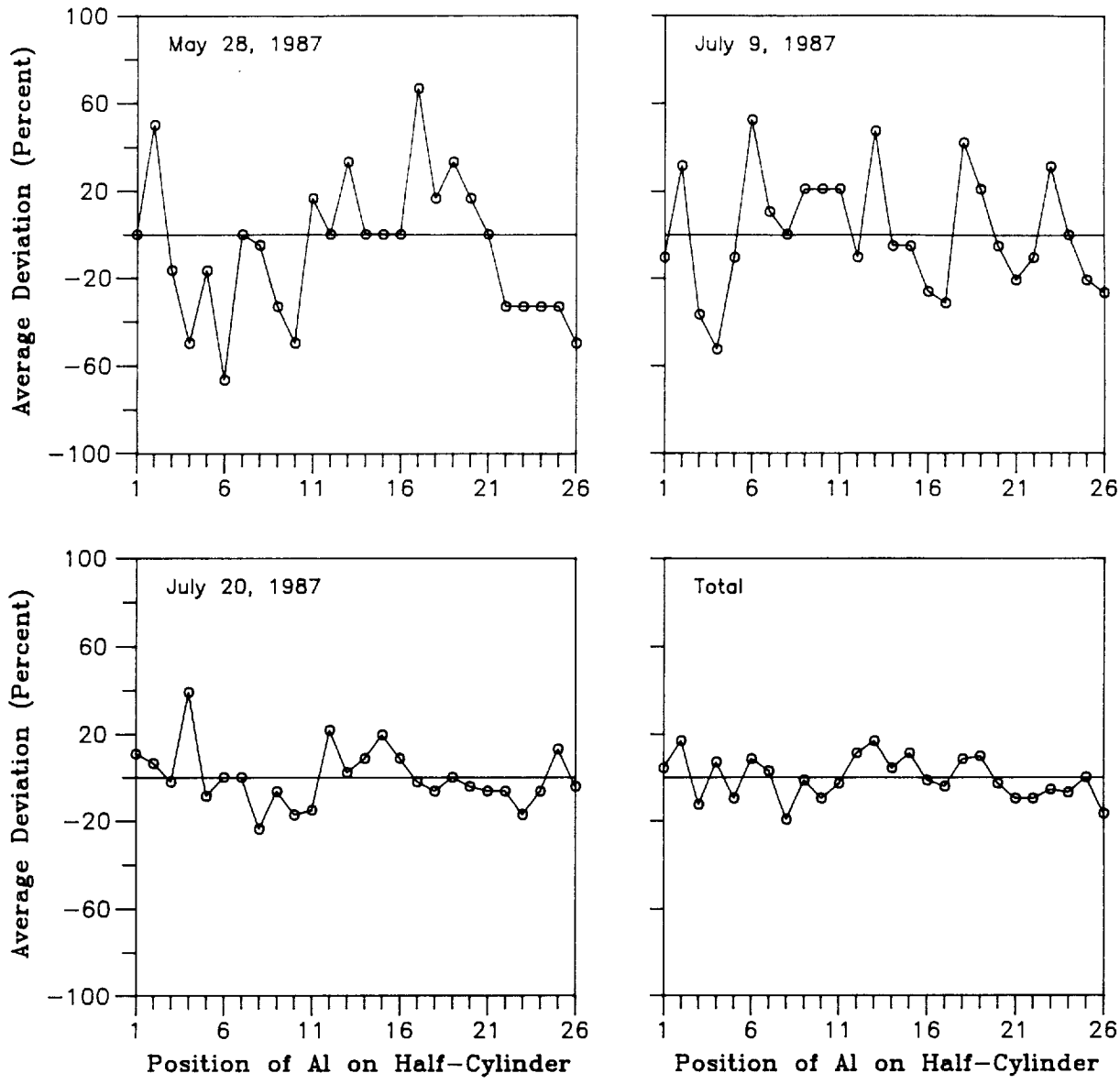

Figure 16: **Percentage deviation from the average number of insects sticking:** Percentage deviation from the average number of insects sticking on each aluminum strip, calculated by Equation 4.1 clearly shows a nonuniform insect distribution across the half-cylinder.

I study and in the results reported by Siochi, *et al.* [25,26]. The probability of mounting a sample at a position of high or a low insect density is large enough so that no reliable comparison between samples can be achieved. It was also noticed that various sizes and varieties of insects were collected on the aluminum strips. Since different sized insects posses different momenta (which is a function of velocity and mass), varying impulse forces would be expected on impact. Also one variety of insect might require a smaller impact force acting on its body to burst open than another. Thus, differences in the sizes and varieties of insects in the environment may also have introduced some additional experimental error.

4.2.2 Results from the Road Tests

The normalized percentages (NP) calculated from the total number of insects collected during the phase I and II studies are given in Table XVII. The results obtained by using thirteen strips for each polymer sample using the modified road test (phase II study) are to be considered more reliable than those obtained with only five strips per sample from the phase I study. This is because statistical errors are reduced by the larger number of runs, and by the new arrangement of using a single type of polymer together with aluminum control strips in the modified road test which reduces some of the experimental errors associated with the nonuniform insect flux across the half-cylinder.

There appears to be at best only small differences in the value of the NP between any of the polymer samples and the aluminum control strips obtained from the phase I and II studies. Some NP values obtained from the phase I study are higher than 100%, while all the NP values obtained from the phase II study are less than or close to 100%. For example, the NP values of Viton^{R} and FCE-E tested in the phase I study are 105% and 121%, respectively, which means there are larger numbers of insects sticking onto these elastomer surfaces than on the aluminum surface. These results from the phase I study are different from those of Wortman [23] who reported that the elasticity of rubber or foam rubber can prevent insects from bursting open and thereby reduce the number of insects sticking. Since elastomers

Table XVII: **Normalized Percentage (NP) of Samples Tested in the Phase I and II Studies.**

Polymer	Phase I (%)	Phase II (%)
FCE–A	82	86
FCE–B	98	88
FCE–C	82	92
FCE–D	90	88
FCE–E	121	78
PU (0.79 mm)	99	—
PU (1.59 mm)	84	—
Neoprene	88	—
Viton^{R}	105	—
SBR–3C	—	97
SBR–7C	—	91
SBR–26	—	79
SBR–17B	—	82

can provide more elasticity than metal (aluminum) surface, the chance of preventing insects from bursting open is greater, therefore fewer insects would be expected to stick onto the elastomers. Perhaps, those NP values higher than 100% obtained from the phase I study are due to the experimental errors introduced during the road tests.

4.2.2.1 Insect Adhesion vs. Elasticity from the Phase I Study

As indicated in Table IX, similar surface energies of the FCE surfaces are obtained from measurements using water/ethanol solutions at different volume ratios. Although the surface energies obtained for neoprene and Viton^{R}are similar to those for the FCE samples, these two samples exhibit higher contact angles for any water/ethanol volume ratio. It is assumed that use of the water/ethanol series with the Owens-Wendt-Young equation is inappropriate for discriminating small differences in solid surface energies. On the other hand, contact angles on the polyurethane surface for any water/ethanol volume ratio are much higher than on the other elastomers. In addition, higher surface energy for the polyurethane sample than for the other elastomers are predicted by the Owens-Wendt-Young equation as expected.

Due to differences in surface energy and modulus of elasticity, all the elastomers tested in the phase I study are divided into three groups. Since the effects of both surface energy and modulus of elasticity are investigated, one of these two parameters must be fixed while the effect of other parameter on insect adhesion is investigated. For example, to study the correlation between the number of insects sticking onto the surface and the modulus of elasticity of the elastomers, their surface energies must be the same or at least insignificantly different. The first group consists of FCE's and the second group consists of neoprene and Viton^{R}. Samples within each group have similar surface energies, but different values of the moduli of elasticity as given in Table XVIII. The third groups is made up of polyurethanes which have identical surface energy but different thicknesses and moduli of elasticity.

Table XVIII: **Modulus of Elasticity (ME) and Normalized Percentage (NP) of Elastomers Tested in the Phase I Study.**

Polymer	ME (kPa)	NP (%)
FCE–A	1,330[1]	82
FCE–B	2,810[1]	98
FCE–C	972[1]	82
FCE–D	1,360[1]	90
FCE–E	2,900[1]	121
PU(0.79 mm)	34,870[2]	99
PU(1.59 mm)	18,030[2]	84
Neoprene	7,790[2]	88
Viton^R	5,930[2]	105

1. Moduli of Elasticity (ME) given are at 200% elongation and were provided by 3M.

2. Moduli of Elasticity (ME) given were calculated from a plot obtained on the Instron. A cross-head speed was 10.0 mm/min.

The NP values of these samples are listed against their moduli of elasticity elasticity in Table XVIII and the NP values of the first group of elastomers are plotted as a function of moduli of elasticity in Figure 17. There is large scatter in the data, and no correlation is obtained between the NP values and the moduli of elasticity. The NP values of the Viton^R (105%) and neoprene (88%) are higher than expected, since the Viton^R sample with a lower modulus of elasticity is expected to reduce the chance of an insect bursting open further than the neoprene sample. Perhaps experimental errors due to a variable insect flux are large enough so that differences in the NP values due to properties of the elastomers become insignificant. The NP value obtained for the 1.59 mm thick polyurethane sample (83%) is lower than for the 0.79 mm thick sample (99%). There are two possible causes for such a difference. One of them is due to the difference in the thickness between two polyurethane samples. Wortman [23] found that as the thickness of the polymer increases, the elasticity becomes more significant, so the number of insect sticking onto a 1.59 mm polyurethane sample is expected to be lower than for a 0.79 mm sample. The other possible reason for such a reduction is due to modulus difference as stated previously. No definite conclusion can be made, and it is probably inappropriate to compare the number of insects sticking on the polyurethane samples as a function of modulus of elasticity.

4.2.2.2 Insect Adhesion vs. Elasticity from the Phase II Study

The FCE and SBR samples tested in this study are divided into two groups. Samples from both groups have similar surface energies but different moduli of elasticity, and are separated into two groups mainly because they are different types of elastomers. The NP values are listed with their water contact angles in Table XIX against their moduli of elasticity. These NP values of the FCE samples are generally less than the ones obtained in the phase I study. Values of the NP are plotted as a function of modulus of elasticity for the FCE and SBR samples in Figure 18. The curve for the FCE sample is similar to the plots presented in Figure 17 for FCE's in the phase I study. However, since these curves are obtained

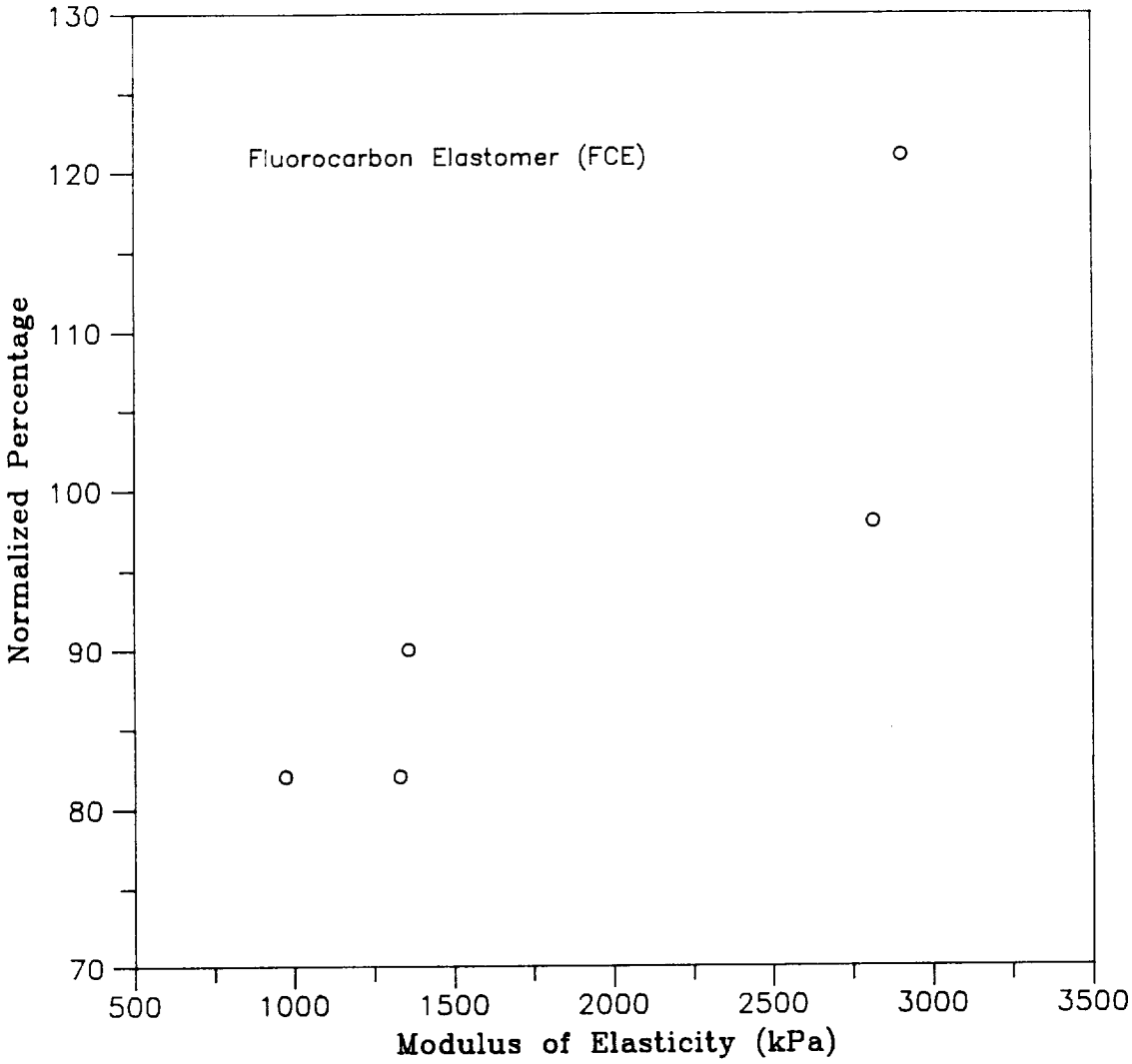

Figure 17: **Normalized percentage (NP) of insects sticking on the FCE elastomers as a function of modulus of elasticity:** There is no correlation between the number of insects sticking on the FCE elastomer surfaces and their moduli of elasticity.

Table XIX: **Modulus of Elasticity (ME) and Normalized Percentage (NP) of Elastomers Tested in the Phase II Study.**

Polymer	θ_{water}	ME (kPa)	NP (%)
FCE–A	92±2	1,330[1]	86
FCE–B	94±1	2,810[1]	88
FCE–C	93±1	972[1]	92
FCE–D	96±1	1,360[1]	88
FCE–E	96±1	2,900[1]	78
SBR–3C	99±3	4,780[2]	97
SBR–7C	95±2	6,420[2]	91
SBR–26	96±2	5,060[2]	79
SBR–17B	95±2	4,890[2]	82

1. Moduli of elasticity given are at 200% elongation and were provided by 3M.

2. Moduli of elasticity given are at 200% elongation and were provided by Fort Belvoir, VA.

from thirteen runs per sample with the new arrangement of sample and control strips, they are probably more reliable than the curves obtained in the phase I study using only five runs per sample. The results again indicate no correlation between the number of insects sticking onto the FCE or SBR surfaces and the modulus of elasticity of these samples. This is possibly because the moduli of elasticity of either FCE or SBR elastomers are too high to give any significant differences in the number of insects sticking onto them. Further discussion of the effect of the modulus of elasticity is given in Section 4.2.4.

4.2.2.3 Results for Teflon^R Tape

The NP value of 30% is obtained for the Teflon^R tape mounted with non-spongy tape, while 27% is obtained for the tape mounted with spongy tape. Thus, the NP value for both the Teflon^R tape mounted with either spongy or non-spongy tape is less than 50%, which is the largest reduction in insect sticking observed for any test in this study. A possible reason for such a large reduction in the number of insects sticking on the both samples is the low-energy surface of the Teflon^R tape, which reduces sticking of the fluid from the impacted insect onto the tape surface. A further small reduction (approximately 7%) of the NP value for the teflon tape sample attached to spongy tape compared to non-spongy tape may be due to the lower modulus of elasticity of the sponge-like mounting tape.

4.2.3 Results from the Phase III Study

Further studies on the effects of surface energy and modulus of elasticity on insect adhesion were done using the air-gun and Drosophila to simulate the insect impact process under controlled conditions. As stated above, the road tests indicated the greatest reduction in the number of insect sticking onto the surface occurred when Teflon^R tape is used, whether supported by a spongy-like mounting tape or by double-stick tape. Since this reduction is assumed to be due to the low surface energy of the Teflon^R tape, the effect of surface

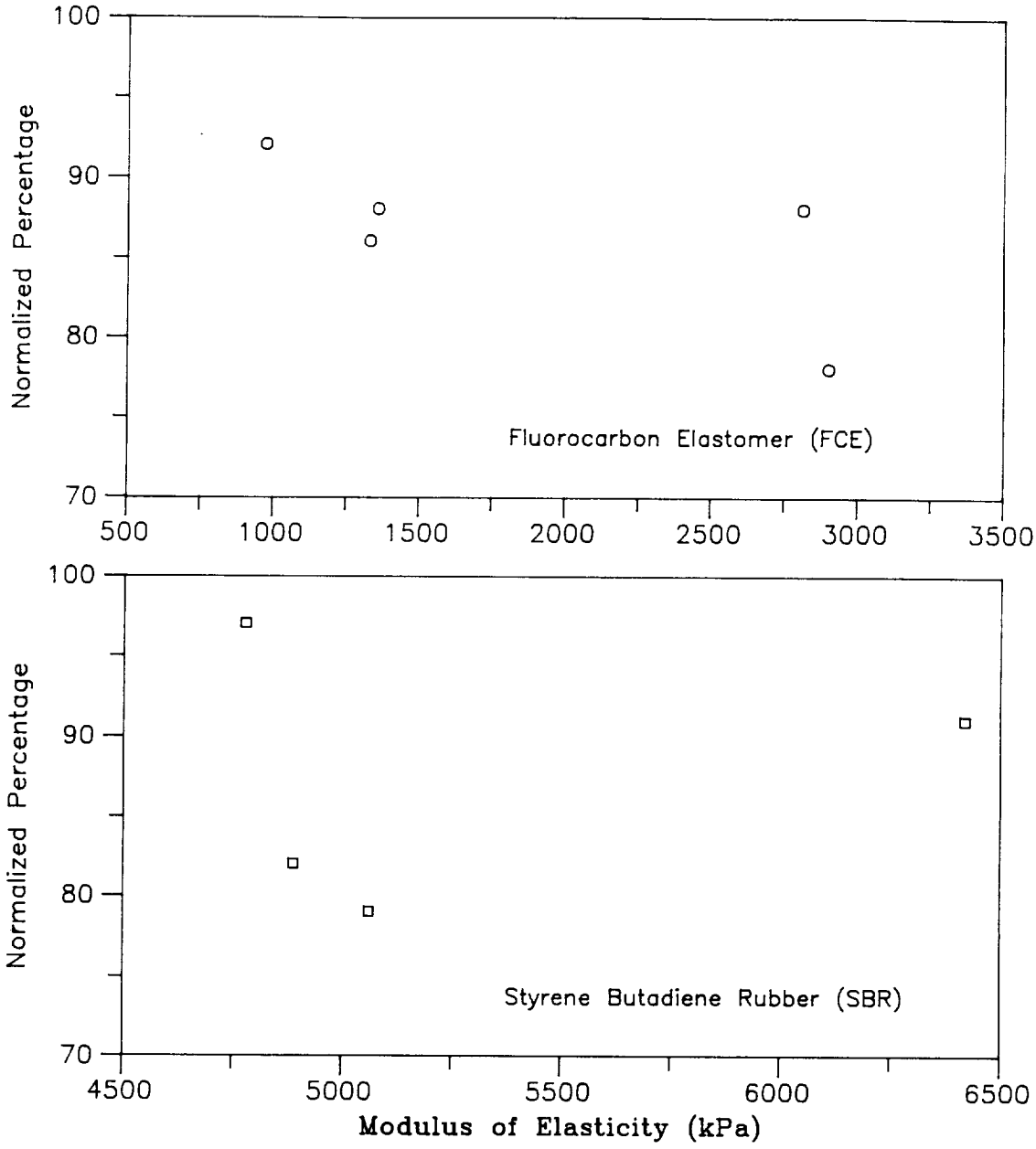

Figure 18: **Normalized percentage (NP) of insects sticking on the FCE and SBR elastomers as a function of modulus of elasticity:** These normalized percentage for FCE (a) and SBR (b) samples are obtained from the road tests by running a single type of sample at a time using a new arrangement of sample and aluminum strips.

energy on insect adhesion was examined in the phase III study with polymer films of various surface energies using the air-gun.

The NP values of sample films tested with the air-gun are listed in Table XX with their surface energies (γ_s) and water contact angles, which are inversely related to the surface energy. While the NP values for a few samples are larger than the 100% for the aluminum control, the NP value of the Teflon^R tape is only 31%, which is similar to the NP value obtained from the phase II study for this sample. The NP values for insects sticking onto fluorinated and non-fluorinated samples are plotted as a function of surface energy in Figure 19. The NP values show a direct relation to the surface energy. That is a larger number of insects stick on a polymer surface with a larger surface energy than one with a lower surface energy. This relation is true for both fluorinated and non-fluorinated polymers. In fact, the correlation between the NP and surface energy is virtually identical for both sets of samples as shown in Figure 19, so that separation of the polymer films into groups is unnecessary.

The NP value is also plotted as a function of water contact angle as shown in Figure 20, and an inverse relation between the NP value and the contact angle is obtained as expected. It is noticed that the NP value for thin coating of Nyebar^R is well fitted on the curve given in Figure 20. Water contact angles are easier to measure than solid surface energies, which require several contact angle measurements using different liquids. The water contact angles of the samples tested in this study may thus be more conveniently used to correlate the NP values with solid surface energy.

The insect impact process onto Teflon^R tape mounted with non-spongy double stick tape and aluminum surfaces was recorded on a video tape, and viewed at slow speed, permitting viewing of the impacting process in slow motion. When an incoming insect impacts on the Teflon^R tape surface and bursts open, its burst-open body sticks on the surface with fluid ejected from within the insect. However, in a large number of cases, the burst-open body is subsequently moved along the surface after a short period of time by the incoming air

Table XX: **Normalized Percentage (NP) of Insect Sticking on Various Polymers with Different Surface Energy (Water Contact Angles)**

Polymer	θ_{water} (degrees)	γ_s (dynes/cm)	NP (%)
PVF	60±2	43.9	108±6
Polyester	65±2	36.5	105±6
Polycarbonate	77±1	33.7	97±7
CTFE	92±2	24.1	96±5
Polyethylene	95±2	22.2	88±4
TEFZEL	95±2	22.1	87±7
Polypropylene	101±3	17.4	84±4
FEP	108±1	15.3	76±4
Teflon^R Sheet	108±2	12.5	71±5
Nyebar^R	109±3	—	68±5
Teflon^R Tape	121±1	5.0	31±1

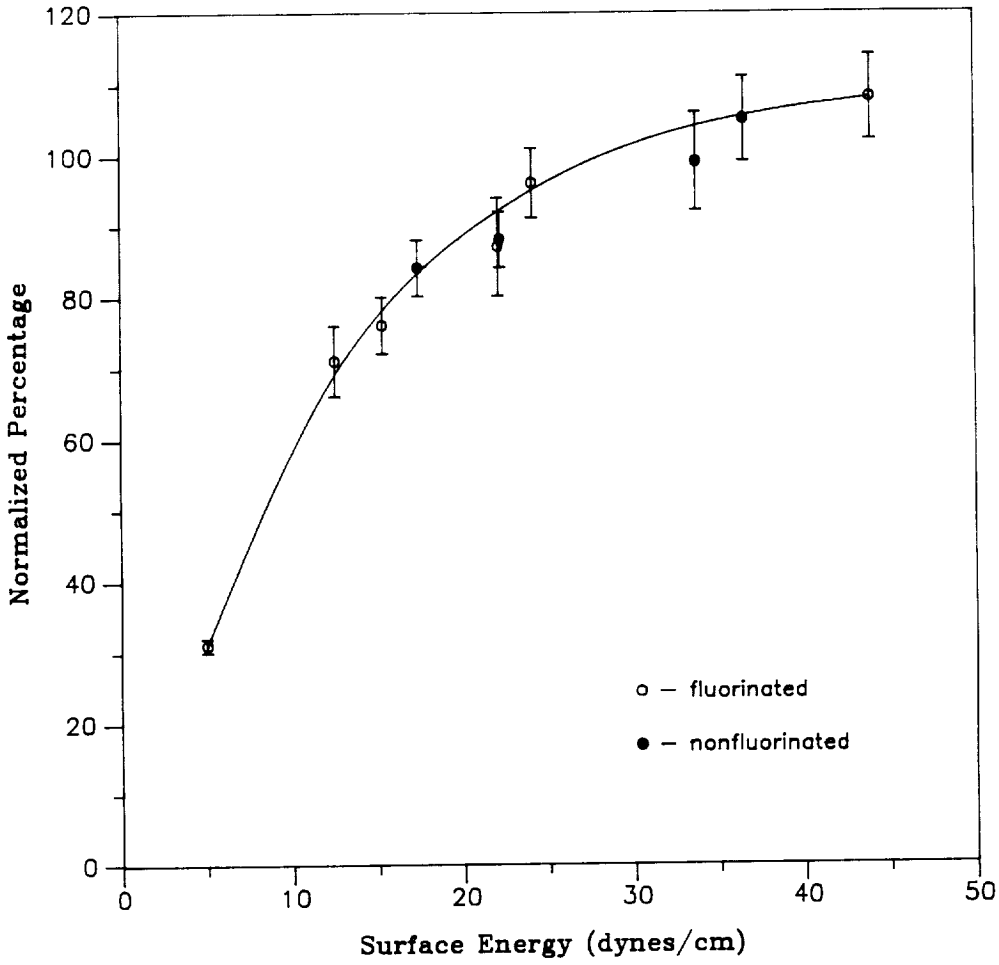

Figure 19: **Normalized percentage (NP) of insects sticking on the polymer films as a function of surface energy:** The NP values show a direct relation to the surface energy for both fluorinated and nonfluorinated sets of samples.

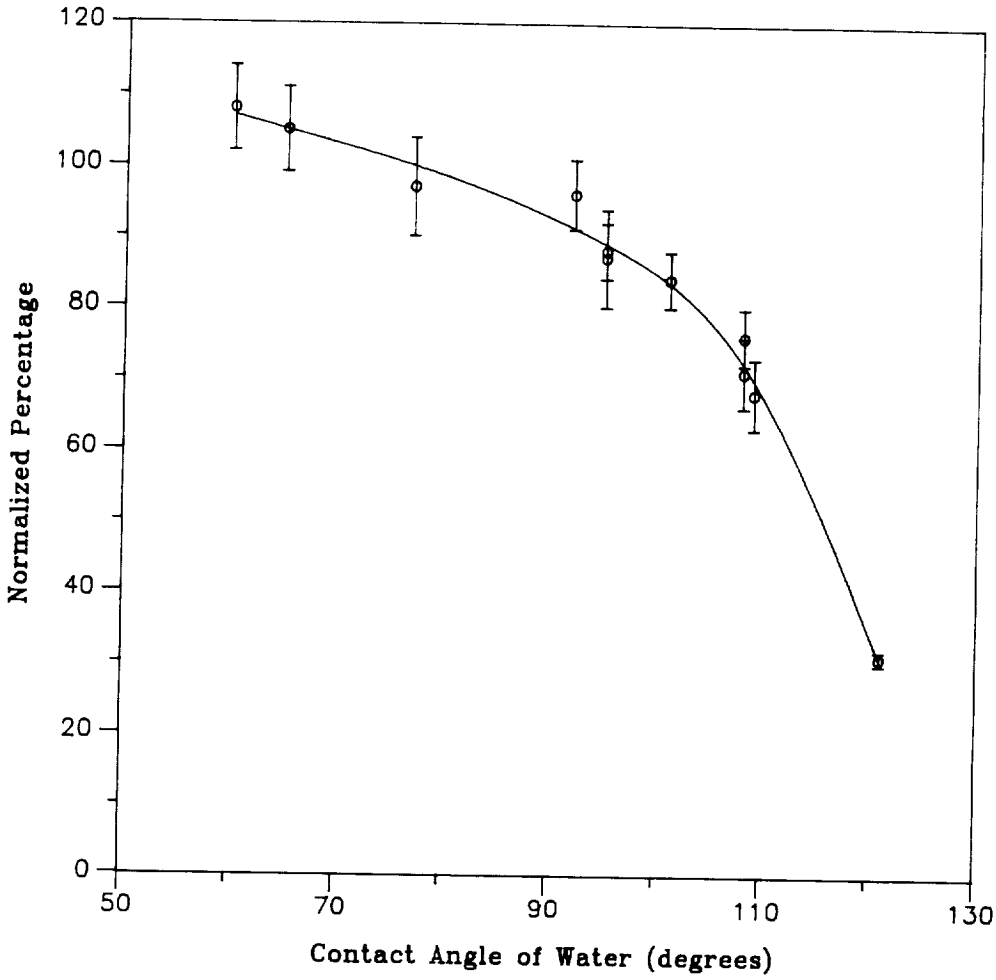

Figure 20: **Normalized percentage (NP) of insects sticking on the polymer films as a function of water contact angle:** There is an inverse relation between the NP value and the contact angle, since contact angle has an inverse relation with surface energy.

flow and finally blown off the surface altogether. This has the effect of reducing the total number of insects that remain adhered to the surface of the Teflon^R tape. On the other hand, all insects which burst open after impacting the aluminum surface remain adhered to the surface and are not easily blown off by the incoming air flow. As a result, a larger number of insects are counted on the aluminum surface after a run is completed than on the surface of Teflon^R tape.

The NP values for the polymers attached to the sample holder with sponge-like mounting tape are listed in Table XXI and plotted as a function of surface energy in Figure 21. The NP values for all samples other than Teflon^R tape are approximately 57±3%. These NP values are less than those obtained for the same samples mounted with the non-spongy double-stick tape. For example, the NP value for the polyester film attached to the sample holder with non-spongy tape is 108%, while the NP value for the same polyester film attached by spongy tape is only 59%. This reduction of the NP value of insects sticking onto polymer film surfaces supported by spongy tape is due to the additional elasticity provided by the spongy tape. The NP value for Teflon^R tape attached onto the sample holder with spongy mounting-tape is only 15%. This value is lower than for other films attached in a similar fashion largely due to the very low surface energy of Teflon^R tape. It should be noted that attaching the Teflon^R onto the sample holder with spongy mounting tape leads to a 50% reduction in the NP value (from NP = 31% to NP = 15%) obtained without the use of the spongy mounting tape. A similar trend was observed in the phase II road test, although the reduction in the NP value obtained by attaching the Teflon^R tape with spongy tape was only 13% (from NP = 31% to NP = 27%). This difference may be due to differences in insect size and type in the two tests and also the duration of the test. Slow motion viewing using video tape of the insect impacting process onto Teflon^R tape mounted with spongy tape show a large number of insects not bursting open while colliding with the sample surface. The incoming air flow then simply blows the insect off the surface.

Similar NP values for all the polymer films with the exception of Teflon^R tape are obtained regardless of differences in their surface energies by using the spongy tape as a supporting

Table XXI: **Normalized Percentage (NP) for Various Polymer Films Mounted on Non-Spongy and Spongy Tapes**

Polymer	With Spongy Tape (%)	With Non-Spongy Tape (%)
PVF	108±7	59±5
Polyester	105±7	60±4
Polyethylene	88±4	61±5
Polypropylene	84±4	57±2
Teflon^{R}Tape	31±1	15±4

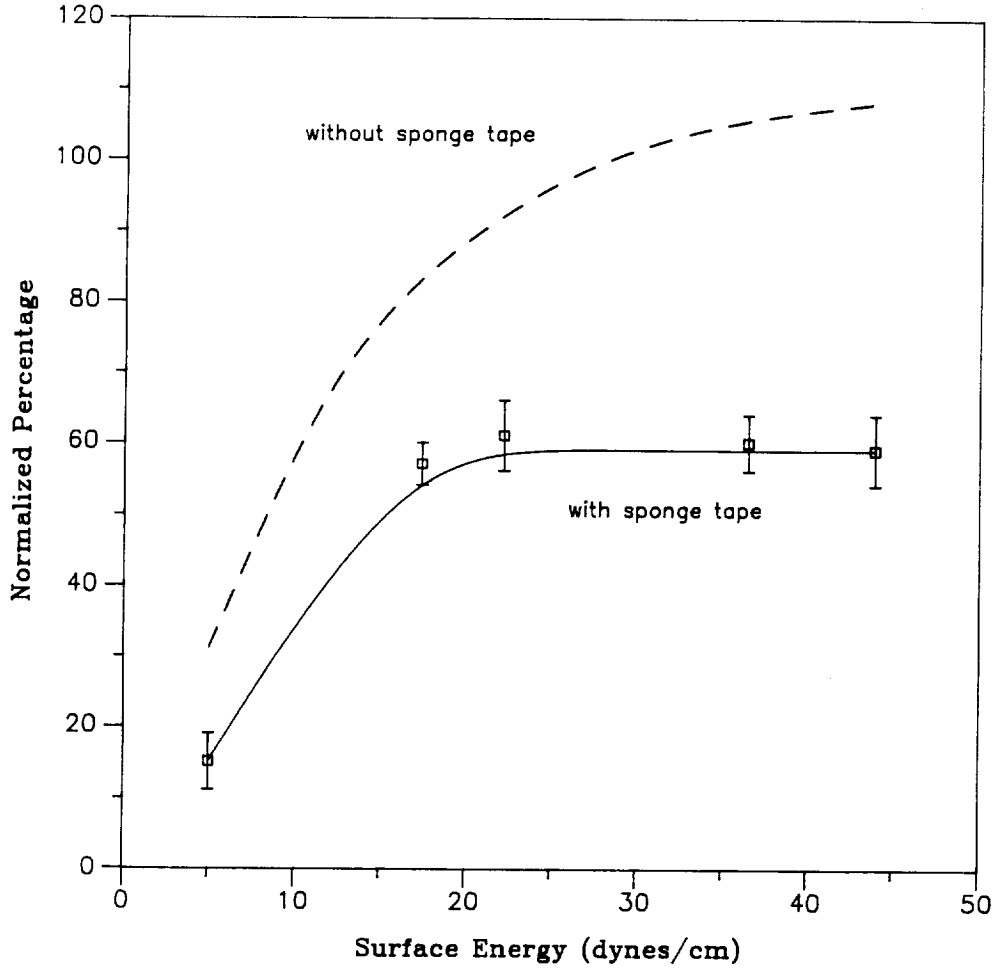

Figure 21: **Normalized percentage (NP) of insects sticking on the polymer films supported by spongy and non-spongy tapes as a function of surface energy:** There is a large reduction on the NP values of insects sticking on polymer film by using spongy tape. This is due to elasticity provided by the spongy tape.

material as stated above. Perhaps this result is obtained because the effect due to the elasticity provided by the spongy tape becomes a dominant factor in preventing insect sticking. On the other hand, both the elasticity of the spongy tape and the low surface energy of the Teflon^R tape affect the number of insects sticking, so that a different NP value (15%) results for the Teflon^R tape. Since the spongy tape is a foam containing a large number of small air-filled holes, its modulus of elasticity is considerably lower than any of the other elastomers tested in this study. To compare differences in the number of insects sticking on the sample surface exclusively due to the elasticity effect, tests were carried out on PVF film supported by additional two elastomers — Viton^R and neoprene. These results may be compared to those obtained in earlier tests using spongy and non-spongy mounting tapes. The surface energy of the exposed PVF surface is fixed at 43.9 dynes/cm. Thus it may be assumed that any observed differences in the NP values from the four cases are due to differences in the elasticity of the mounting materials. The elasticity of the thin non-spongy tape is sufficiently small that its effect on the insect impacting process may assumed to be negligible, so that in this case, the PVF film could be considered as mounted onto bare aluminum. The results from this study are listed in Table XXII. There are large differences in the NP values for the PVF film depending on the mounting material used. As expected, the smallest NP value (59%) is obtained for the sample prepared with the spongy tape, while the largest value (108%) is obtained with the non-spongy tape. Intermediate values are obtained with neoprene and Viton^R which posses moduli of elasticity lower than that of the non-spongy tape on an aluminum surface, but higher than the spongy tape. The results also indicate that a significant difference in the number of insects sticking can only be achieved for elastomers with fairly low moduli of elasticity. This would be the case if the reduction in the number of insects sticking onto the surface (or the NP value) is only a weak function of the modulus of elasticity, until a reasonably low modulus of elasticity is reached. A further discussion of the effect of elasticity on the mechanics of insect impact is given in the following section.

Table XXII: **Normalized Percentages (NP) for the PVF Film Mounted on Various Materials.**

Material Used	NP (%)
Non-spongy tape	108±7
Viton^{R}	83±8
Neoprene	77±3
Spongy tape	59±5

4.2.4 Discussion of Effects of Surface Energy and Elasticity

The fact that insects are observed to stick on all surfaces used in the road test is *prima facie* evidence of molecular contact (adhesion) between the insect fluid and the surface. The high velocity of incoming air has two effects on sticking, namely, increasing the rate of drying of the insect fluid after the insect has burst, leading to increased viscosity, as well as forcing the insect fluid to spread over the surface. The reason for the observed change in the sticking of insects due to the surface energy (for example, Teflon^{R}tape compared to polyester or PVF) can be explained as follows. Suppose an insect impacting on the sample surface at high velocity during the road test bursts open. The insect fluid will be wetting or nonwetting depending on the surface energy of the solid surface. Drops of insect liquid on low energy surfaces will have reduced wettability, and will therefore require a larger force to spread over the surface so that the contact area with the solid is small. Thus, in such a surface the drops of insect liquid tend to ball up. Therefore the chance of an insect body being blown off the surface by the incoming airflow is greater, thereby reducing the number of insects that remain stuck onto the polymer surface over a period of time.

The effect of polymer elasticity on the mechanism of the insect impact process may be best explained by considering an insect of mass m_i approaching the sample surface at a constant velocity of v_i. The momentum of the insect just prior to impact is $m_i v_i$ and its kinetic energy is $m_i v_i^2/2$. The mass of a typical fruit fly (Drosophila) is approximately 0.2 mg. At an approach velocity of 60 mph or 26.7 m/sec, the insect posses a momentum of 5.34×10^{-6} N/sec and a kinetic energy of 1.43×10^{-4} J. When the insect impacts the sample surface, it is decelerated to zero velocity (and hence zero momentum). Simultaneously, the kinetic energy of the insect is dissipated. If the solid surface is not easily deformable (it has a high modulus of elasticity), the energy possessed by the incoming insect will be insufficient to significantly deform the surface. Thus, the insect will be rapidly decelerated. The impulse force that the insect exerts onto the surface on impact is equal to the rate of change of momentum during the collision between the insect and the surface. By Newton's

third law of motion, an equal but opposite force is also simultaneously exerted upon the insect. Impulse forces are large particularly if the duration of the collision (which equals the time taken for the insect to decelerate to zero velocity) is small. For example, if the collision lasts about 1 ms, the force exerted onto the insect is 5.34 X 10^{-3} N assuming an incoming velocity of 60 mph. This is a considerable force on such a small organism. The cross-sectional diameter of a fruit fly is approximately 0.7 mm, so that its cross-sectional area is 3.85 X 10^{-7} m^2. When the insect collides end-on with the surface, a pressure of 14,000 Pa or 2 psi is exerted on the exoskeleton of the insect. If the collision lasts 0.1 ms, this pressure increases to 20 psi. If this pressure exceeds the maximum pressure that the exoskeletonal structure of the insect is capable of withstanding, the insect will burst open. This analysis clearly shows that the duration of the collision strongly influences the force and hence the pressure exerted on the insect exoskeleton.

Suppose the insect impacts the surface of a polymer with a low modulus of elasticity. Its kinetic energy of impact is fixed at $m_i v_i^2/2$. Since the polymer has a low modulus of elasticity, this amount of kinetic energy is capable of deforming the surface of the polymer. As the polymer surface deforms, it prolongs the collision. That is, the rate of deceleration of the insect is lower. As a consequence, the rate of change of momentum and hence the force exerted on the insect are lower. For instance, if the collision lasts 0.01 sec instead of 0.001 sec; the impulse force exerted on the insect is of the order of 0.5 X 10^{-3} N, and the corresponding pressure exerted on the insect skeleton is only 0.2 psi. If the force and pressure applied to the insect exoskeleton is reduced to a level below that which causes its rupture, the insect will not burst upon impact. Thus only a polymer with a sufficiently low modulus of elasticity is capable of preventing insects from bursting open on impact. It is also worth noting that the orientation of the insect on impact will vary the pressure exerted on its skeleton, since the area over which the impact force acts is varied. This together with the fact that the strength of the exoskeleton varies over the body of the insect might explain why a few insects do burst open on a sponge-tape backed polymer film.

Chapter 5

Conclusions

Fuel efficiency, which has been a continuing concern of commercial airlines, is accomplished in part by a wing design that will reduce drag on aircraft. Efficiency, however, is decreased significantly by the build-up of insect debris on the leading edge of airfoils during the ground run, climb, and landing. Thus, insect debris roughens airfoil surfaces; the laminar flow over the wing is replaced by turbulent flow, resulting in increased drag and hence, lower fuel efficiency.

The feasibility of reducing the number of insects sticking to the airfoils by coating the leading edges with polymers is investigated in this study. The effects of the surface energy and elasticity of the polymer on insect adhesion were examined, and a better understanding of the insect-sticking mechanism on modified wing surfaces has been achieved.

The impact of insects on modified airfoil surfaces was achieved in a laboratory environment by the use of a device which is capable of accelerating insects up to speeds of 170 km/hr, and impacting them onto a stationary target. The device is basically an air-gun which consists of a PVC pipe, T-connector, and nozzle. The PVC pipe is sufficiently long that a uniform velocity distribution is obtained at its exit. A rectangular plexiglas duct is placed

at the end of the PVC pipe to prevent the air flow exiting the circular pipe from diverging into the environment. The target consists of polymer samples in the form of thin strips, adhesively bonded onto a wide aluminum strip, mounted onto a sample holder which is in the shape of the leading edge of an airfoil. The sample holder is placed at the exit end of the rectangular duct, and at the center of its cross-section.

A small flow rate of highly compressed air is passed through the nozzle, and the high degree of expansion and high velocity of the air exiting the nozzle creates a suction behind the nozzle which in turn induces a large inflow of air from the surroundings through the feed chute. This large volume of air is accelerated as it flows past the nozzle, creating a high velocity flow of air in the downstream section of the pipe. Live fruit flies (Drosophila) introduced into the feed chute are drawn in with the air and also accelerated to a high velocity, finally impacting the target placed in the rectangular duct.

A direct relation between the number of insects sticking on sample surfaces and their surface energies was obtained. When incoming insects impact onto a polymer surface at high velocity, they may burst open. The liquid from within the insect acts as an adhesive which bonds the insect debris to the surface. If the surface energy of the polymer is low (low surface wettability), the liquid will not spread, but instead will ball up providing poor adhesion between the insect debris and the surface. Thus the number of insects sticking on a lower energy surface is less than on a higher energy surface.

In addition to surface energy, the elasticity of the polymer also plays a part in determining the number of insects which stick to the surface. A direct relation between the number of insects sticking onto sample surfaces and their moduli of elasticity was obtained. Elastomers with a low modulus of elasticity are capable of greater deformation so that the deceleration of the insect is lowered. As a consequence, the rate of change of momentum is lower and the force and pressure exerted on the body of the insect is reduced if it impacts onto a material with a low modulus of elasticity. This lessens the chance of bursting the insect exoskeleton thereby reducing the number of insects sticking onto the sample surface. Video examination

shows in fact, that fewer insects that impact onto a sample with a low modulus of elasticity do burst open.

Chapter 6

Recommendations

The following are recommended for further study.

1. The momentum of an insect with given mass impacting on the target surface largely depends on the velocity of the insect, and this momentum determines the pressure exerted on the exoskeleton of the insect. Since bursting open of the insect body is determined by this pressure, it is logical to assume that changes in the impact velocity of the insect will alter the number of insects sticking on the target surface. The effect of insect velocity on the number of insects sticking on sample elastomers and polymer films may be investigated by varying air velocity in the air-gun.

2. The effect of the elasticity of elastomers may be studied more extensively using elastomers with a wide range of moduli of elasticity than used in this study.

3. Wortmann [23] found that as the thickness of rubber increases, elasticity becomes more effective even at the high velocities investigated. The effect of the thickness of the elastomers is recommended as a variable for further investigation.

4. The contact area between the sample surface and the burst-open insect body varies depending on the surface energies of the polymers. It might be possible to measure

this contact area as follows. Strips of translucent or transparent polymer films of various surface energies are attached to a strip of the clear vinly acetate using the doulbe stick tape, and affixed to the sample holder as described in Chapter 3. The areas between the burst-open insect bodies and the polymer surfaces will be visible from the bottom surface -unused surface of the vinyl acetate if the sample is held against a light source. Using image analysis, the contact areas of the burst-open insect body on polymer films of different surface energies may be determined.

Bibliography

[1] Povinelli, F. P., J. M. Klineberg, and J. J. Krame, *Astronautics & Aeronautics*, **14** (1976), 18.

[2] Bauchspies, J., F. Hopkins, and L. Kaplan, *NASA CR-169116* November 1980.

[3] James, R. L. and D. V. Maddalon *NASA TM-85749*, March 1984.

[4] James, R. L. and D. V. Maddalon *Aerospace America*, **22**, (1984), 54.

[5] Cotta, R., *Aviation*, January 1980, 12.

[6] Wagner, R. D. and M. C. Fisher, *Aerospace America*, **22**, (1984), 72.

[7] Luers, J. K., *Astronautics & Aeronautics*, **26**, (1983), 54.

[8] Carmichael, B. H., *NASA CR-152276*, May 1979.

[9] Maresh, J. L. and M. B. Bragg, *AIAA 2nd Applied Aerodynamics Conference*, Seattle, Washington, August (984), 1.

[10] Peterson, J. B. and D. F. Fisher, *NASA CP 2036*, 1978.

[11] Howard, R. W., *Ann. Rev. Entromology*, **27**, (1982), 149.

[12] Evered, D., M. O'Connor, and J. Whelan ed. *Neuropharmacology of Insects*, Ciba Foundation Symposium 88, 1982.

[13] Rees, R. R., *Insect Biochemistry*, Chapman and Hall Ltd., London, 1977.

[14] Andersen, S. O., *Ann. Rev. Entomology*, **24**, (1979), 29.

[15] Hepburn, H. R. and I. Joffe, in *Insect Integument*, Ed. Hepburn, H. R., Elsevier Scientific Publishing Company, Amsterdam, (1976), 207.

[16] Hepburn, H. R. and I. Joffe, *J. Insect Physiol.*, **20**, (1974), 497.

[17] Hepburn, H. R. and H. D. Chandler, *Comp. Physiol.*, **109(B)**, (1976), 177.

[18] Hepburn, H. R. and H. D. Chandler, *J. Insect Physiol.*, **22**, (1976), 221.

[19] Hepburn, H. R. and D. C. Roberts, *J. Insect Physiol.*, **21**, (1975), 1741.

[20] Hepburn, H. R. and I. Joffe, *J. Insect Physiol.*, **20**, (1974), 631.

[21] Freeman, J. A. *J. Am. Ecol.*, **14**, (1945), 128.

[22] Gray, W. E. and H. Davies, *Aeronautical Research Council Reports and Momoranda*, London, (1952), paper 2485.

[23] Wortmann, F.X., *NASA TM-77419*, March 1984.

[24] Gratzer, L. B. and D. G. Falvy, in *CTOL Transport Technology-1978*

[25] Siochi, E. J., N. S. Eiss, D. R. Gilliam, and J. P. Wightman *Journal of Colloid and Interface Science*, **115**, (1987), 346.

[26] Siochi, E. J. *A Fundamental Study of the Sticking of Insect Residues to Aircraft Wings*, M.S. Thesis, Virginia Polytechnic Institute and State University, Blacksburg, Virginia, (1985).

[27] Bird, R. B., W. E. Stewart, and E. M. Lightfoot, *Transport Phenomena*, John Wiley & Sons Inc., New York, 1960.

[28] Welty, J. R., C. E. Wicks, and R. E. Wilson *Fundamentals of Momentum, Heat, and Mass Transfer*, John Wiley & Sons Inc., New York, 1984.

[29] Zisman, W. A., in *Contact Angle, Wettability and Adhesion - Advances in Chemical Series 43*, Eds. Gould, R. F., American Chemical Society, Washington D.C., (1964), 1.

[30] Shafrin, E. G. and W. A. Zisman, *J. Phys. Chem.*, **64**, (1960), 519.

[31] Bernett, M. K. and W. A. Zisman, *J. Phys. Chem.*, **63**, (1959), 1241.

[32] Dann, J. R., *J. Colloid and Interface Science*, **32**, (1970), 302.

[33] Owens, D. K. and R. C. Wendt, *J. Appl. Polymer Sci.*, **13**, (1969), 1741.

[34] Owen, M. J., *J. Coatings Technology* 53, August, 1981.

[35] Shaw, D. J., *Introduction to Colloid and Surface Chemistry*, Butterworths & Co. Ltd., Boston, 1985.

[36] Adamson, A. W. *Physical Chemistry of Surfaces*, John Wiley & Sons, Inc., New York, 1982.

[37] Kane, P. F. and G. B. Larrabee Ed., *Characterization of Solid Surfaces*, Plenum Press, New York, 1974.

[38] Sherwood, P. M., *The Royal Soceity of Chemistry*, Burlington House, London, 1985.

[39] Hercules, D. M. and S. H. Hercules, *Analytical chemistry of Surfaces: Part II. Electron Spectroscopy*, J. Chemical Education,**61**, (1984), 483.

[40] Relley, C. N. and D. S. Everhart, *Applied Electron Spectroscopy for Chemical Analysis*, Eds. Windawi, H. and F. F. Ho, John Wiley & Sons Inc., New York, (1982), 105.

[41] Briggs, D., in *Practical Surface Analysis*, Eds. Briggs, D. and M. P. Seah, John Wiley & Sons Inc. New York, 1983.

[42] McIntyre, N. S., in *Applied Electron Spectroscopy for Chemical Analysis*, Eds. Windawi, H. and F. F. Ho, John Wiley & Sons Inc. New York, (1982), 89.

[43] Windawi, H. and C. D. Wagner, in *Applided Electron Spectroscopy for Chemical Analysis*, Eds. H. Windawi and F. F. Ho, John Wiley & Sons Inc., New York, (1982), 191.

[44] Thomas III, J. H. in *Applied Electron Spectroscopy for Chemical Analysis*, Eds. H. Windawi and F. F. Ho, John Wiley & Sons Inc., New York, (1982), 37.

[45] Jastrzebski, J. D., *The Nature and Properties of Engineering Materials*, John Wiley & Sons Inc., New York, 1977.

APPENDIX A

CALCULATION OF BUG VELOCITY IN AIR GUN

The purpose of this calculation was to determine if the bug was accelerated to the air velocity in the distance it traveled from the point where it was introduced into the air stream to the airfoil. This distance was 3.81 m. To perform this calculation, several assumptions were made.

1. The fruit fly was modeled as a sphere with a diameter d = 1 mm.
2. The mass, m, of the fruit fly was 0.1 mg.
3. The kinematic viscosity, η, of air was 15.75 $(10)^{-6}$ m^2/s.
4. The air stream velocity was 15.23 m/s.
5. The air density, ρ, was 1.1766 kg/m^3.

When the bug was injected into the air stream, its velocity relative to the air stream was 15.23 m/s. The Reynold's number R_e for this velocity is:

$$R_e = \frac{Vd}{\eta} = \frac{15.23 \text{ m/s } 10^{-3}\text{m}}{15.75\ (10)^{-6}\ \text{m}^2/\text{s}} = 967$$

The drag coefficient C_D for this R_e on a sphere is 0.5. As the insect is accelerated, the relative velocity and hence the R_e decrease. Because the C_D rises as R_e decreases, a calculation based on a constant C_D will give a lower bound on the velocity of the insect when it reaches the airfoil.

The drag force F_D is given by

$$F_D = C_D \left(\frac{\pi d^2}{4}\right) \left(\rho \frac{V^2}{2}\right)$$

where $V = V_a - V_b$

a = air

b = bug

$$F_D = \frac{0.5\ \pi\ 10^{-6}\ m^2\ 1.1766\ kg/m^3\ (15.23\ m/s - V_b)^2}{8}$$

$$F_D = 0.924\ (10)^{-6}\ (15.23 - V_b)^2 \qquad \ldots 1$$

The dynamic model for the acceleration of the bug is Newton's second law

$$F_D = m\ \dot{V}_b = 10^{-7}\ kg\ \dot{V}_b \qquad \ldots 2$$

Equation 2 is solved for $\dot{V}_b$ and Eq. 1 is substituted for F_D

$$\dot{V}_b = 9.24\ (15.23 - V_b)^2 \qquad \ldots 3$$

Equation 3 is nonlinear and was solved by a Runga-Kutta numerical integration using a code Personal Simulation Language (PSL), developed at VPI&SU.

The solution to Eq. 3 is shown in Fig. A1. The dotted lines show that when the bug has traveled 3.8 m, its velocity is 14.8 m/s which is 97 percent of the freestream velocity. Because the drag coefficient was assumed to be constant, this velocity represents a lower bound of the actual bug velocity. Consequently, the bug velocity can be assumed to be equal to the air velocity with less than 3 percent error.

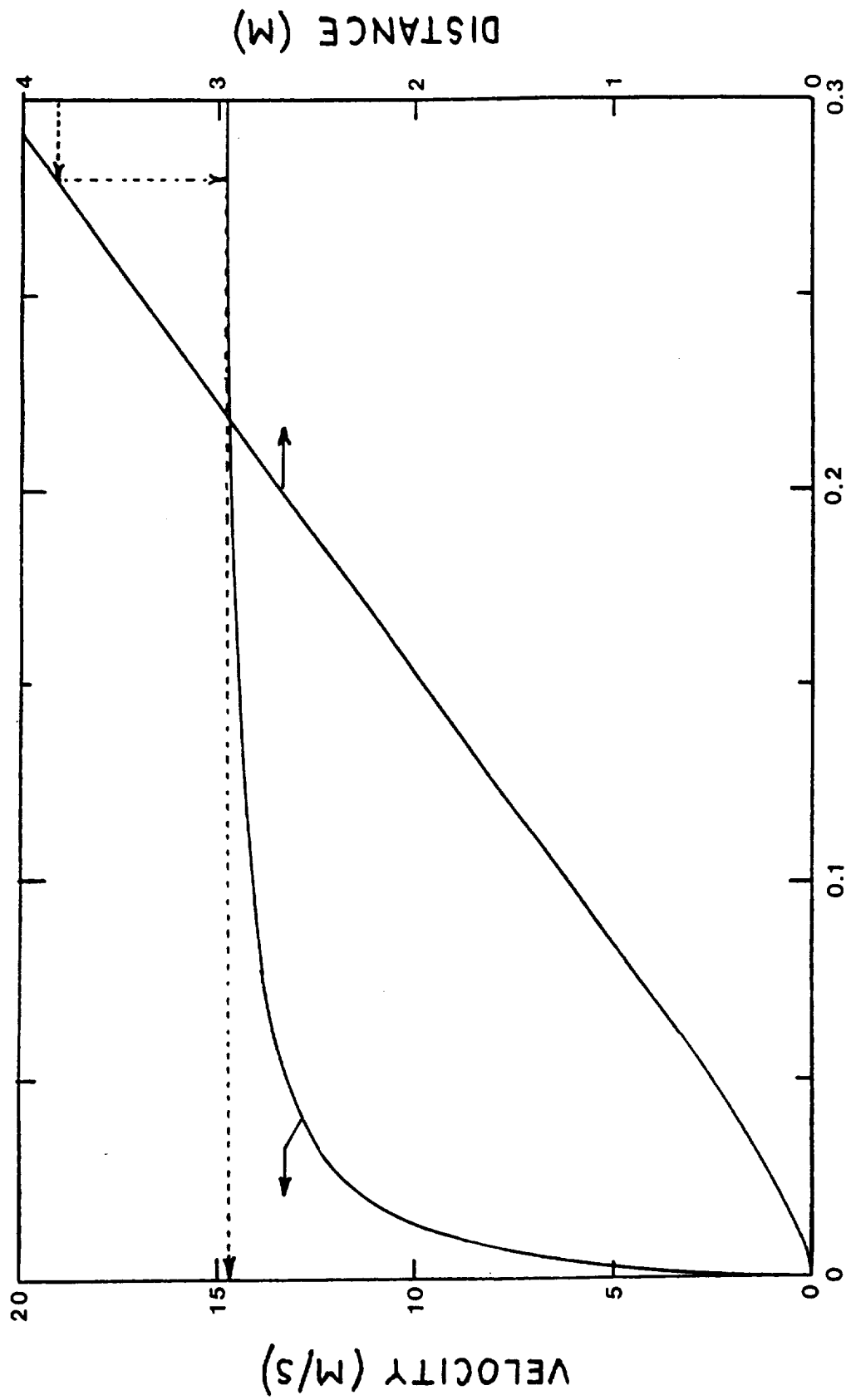

Fig. A1. Bug velocity and distance traveled measured from the time that the bug was injected into air stream with a velocity of 15.23 m/s. Dotted line shows bug velocity when it has traveled 3.8 m.